QA: L

Level 4 Milestone SPY289M4
June 30, 1998
Version 1.0
Yucca Mountain Site Characterization Project

Thermo-Hydro-Chemical Predictive Analysis For The Drift-Scale Heater Test

Eric Sonnenthal, Nicolas Spycher, John Apps, and Ardyth Simmons

Lawrence Berkeley National Laboratory

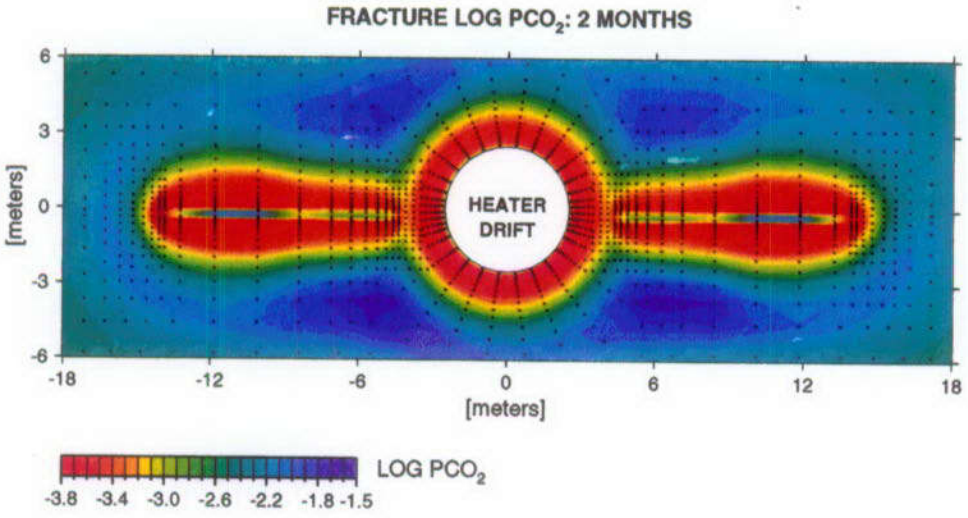

Earth Sciences Division
Lawrence Berkeley National Laboratory
One Cyclotron Road MS 90-1116
Berkeley, CA 94720

1. INTRODUCTION

This report presents a predictive analysis of the geochemical and isotopic alteration of minerals, fluid, and gas accompanying the underground Drift-Scale Heater Test (DST) begun in December 1997. The aim of this analysis is to incorporate the important geochemical and physical phenomena in a numerical model, using and assessing the current information on pore-water chemistry, mineralogy, thermodynamic and kinetic data, and heater test conditions. This work represents an initial effort to understand the system behavior, and the results should not be used by YMP researchers to provide quantitative estimates of the processes investigated. The DST will operate over a period of eight years; as data are collected the models and understanding of the system will undergo refinement and reevaluation. In overall terms, our objective is to provide a better understanding of the coupled thermo-hydrological-chemical (THC) system that could be applied with a higher level of confidence to constrain the behavior of the proposed repository for a period of ten thousand years or more.

In such a complex, highly coupled system, there are many variables that are only known approximately or not at all (e.g., thermodynamic data, rates of dissolution and precipitation, nucleation kinetics, reactive surface areas and surface properties, and mineral heterogeneity) in addition to uncertainties in the hydrological properties of fractured tuff. Therefore it is necessary to consider these analyses to be sensitivity studies along the path of understanding the system behavior. Given these caveats, constraints can be applied so that once geochemical data are collected, they can be used to obtain the overall rates of reaction, even if some of the detailed reaction parameters are unobtainable. One example we present is the use of Sr isotopic ratios to estimate the shift in the $^{87}Sr/^{86}Sr$ isotopic ratio in water as a function of the dissolution of the anorthite component in feldspars.

A much better constrained aspect of coupled THC processes is the behavior of heat, fluid, and water vapor transport, in the absence of strong effects on permeability and porosity, accompanying the DST. Our model grid, input thermal and hydrological parameters, and boundary conditions are those developed for the thermo-hydrological model of the DST presented by Birkholzer and Tsang (1997). Their work, in turn, derives important parameters for unsaturated zone flow in matrix and fractures (e.g., Bandurraga and Bodvarsson, 1997; Sonnenthal et al., 1997a) from the site-scale unsaturated zone (UZ) flow model, and of course from various data and insights developed by others for the Yucca Mountain Project. Thus, the philosophy of this work is to combine the current capabilities regarding the physical behavior of the system with a conceptual model and numerical code to study geochemical effects on the system and the possible coupling to their thermohydrology.

The initial pore-water geochemistry is an important starting point in the simulation of water-rock interaction. Because no analyses have been made in the DST area, we present an analysis of the pore water geochemistry at Yucca Mountain and make an estimate of what could be a representative or average, pore-water chemistry for the Topopah Spring welded tuff. As for the thermo-hydrology, we build on the work presented to understand the controls on the ambient pore-water chemistry in the mountain (Apps, 1997; Yang et al., 1996a,b) and models for the strontium isotopic effects observed (Sonnenthal et al., 1997b).

Fundamental inputs to the numerical model are the thermodynamic and kinetic data. Here we present a new analysis of some of the relevant thermodynamic data for minerals under the conditions expected for the DST. We also build strongly on the kinetic and thermodynamic data (Hardin, 1998), fundamental reaction-transport experiments (Johnson et al., 1997a,b) and analysis of the geochemical system expected for the near-field environment and for the Single Heater Test (Glassley et al., 1997).

As of the start of this project in late 1997, there were no available numerical codes that could handle a general problem of multicomponent and multiphase transport, heat, equilibrium and kinetic mineral-water reaction, adsorption and exchange, and gas species transport for 2-D and 3-D dual-permeability problems for an arbitrary number of chemical species and mineral phases. Our work has involved the adaptation, enhancement, and testing of the TOUGHREACT code (Tianfu Xu and Karsten Pruess, 1997; 1998), in order to handle these important aspects of the DST, Single Heater Test, and the repository-induced THC processes. To build confidence in the code and our conceptual model of reaction-transport processes, we present several comparisons to experiments and to other modeling results under equilibrium and kinetic conditions. We also present sensitivity studies on the geochemistry of boiling systems to help us in our understanding of the DST simulation results.

Important aspects of the problem and numerical code are still being implemented and tested, such as a module to couple the feedbacks to flow via porosity, permeability changes in fracture and matrix, and the reverse feedback to the grain sizes, reactive surface areas, and textural relationships. This, along with an overview of our accomplished and planned work, is presented in the following section.

2. WORK COMPLETED, ONGOING AND PLANNED

2.1 Purpose and scope of this report

This report provides a predictive analysis of thermohydrochemical (THC) processes in the DST. The work was conducted under WBS 1.2.3.14.2 in Work Package 123E2275M2. Under this directive, the pre-test predictions are the first step in a comprehensive analysis to refine and update model predictions related to geochemistry/mineralogy-petrology data from the DST.

This section presents an overview of the tested numerical code capabilities (verification and validation), data assessed, and simulations undertaken.

2.1.1 Major code capabilities of TOUGHREACT and use for this project

2.1.1.1 Numerical Code

- Heat, fluid, water vapor transport (identical to Q-version of TOUGH2 v 1.11 EOS3).
- Dual permeability formulation (transport, flow, and diffusion between fractures and matrix, with separately defined mineral proportions and properties in each continuum);
- Equilibrium, kinetic, or mixed reactions for precipitation and dissolution;
- Any number of primary and secondary aqueous species (tested 13 primary, 29 secondary);
- Any number of minerals (tested 20 minerals);
- Diffusion and advection of species in aqueous and gas phases;
- Development and incorporation of a new thermodynamic database;
- Incorporation of different rate laws for precipitation and dissolution;
- Adsorption and ion exchange (implemented but not considered in this report);
- Consideration of CO_2 transport in gas phase. O_2 and redox have been considered for problems related to supergene enrichment (Xu et al., 1998a). Gas phase species currently considered in equilibrium with fluid.
- Isotopic ratios in fluid; calculation of $^{87}Sr/^{86}Sr$ ratio in pore fluid.

2.1.1.2 Data Analysis

- Pore-water geochemistry;

- Thermodynamic data;
- Kinetic data;
- Ambient mineralogy.

2.1.1.3 Verification and Validation

- Verification by comparison to analytical solutions and other simulators for equilibrium and kinetic conditions at 25°C (Xu, 1996; Xu et al., 1998a, Xu et al., 1998b);
- Comparison to SOLVEQ/CHILLER equilibrium model result (Reed, 1982; Spycher and Reed, 1992) under heating and boiling conditions;
- Modeled quartz and TSw tuff plug flow reactor experiments by Johnson et al. (1997a).

2.1.1.4 Model Simulations

Using the exact thermohydrological predictive model (mesh, thermohydrologic properties, initial and boundary conditions, etc.) from the DST simulation by Birkholzer and Tsang (1997) we made:

- Simulations of mineral phases, proportions, fluid, and gas compositions in fractures and matrix (dual permeability) as a function of space and time in 2-D;
- Estimates of porosity changes—currently no coupling of porosity and permeability changes to flow field;
- Simulation of the Sr isotopic ratio in the fluid.

Model results are presented here for different time periods up to the full eight year planned heating and cooling phases of the DST. Because of the complexity of the geochemical systems and their sensitivity to numerical errors, transport effects, and thermodynamic/kinetic input data, the results should be considered as exploratory and will require further study to confirm whether they are representative of processes in the DST.

2.1.2 Model developments in progress

- Coupling porosity and permeability changes to the flow field, updating reactive surface areas and crystal morphology in fracture and matrix continua;

- Completing a model for Sr isotopic ratios to include both exchange and precipitation effects;
- Evaluating the effects of boiling, condensation and transport on oxygen and deuterium isotopic ratios;
- Evaluating and testing conceptual models for chemical transport between fractures and matrix;
- Refining mineral distributions and heterogeneity in fractures and matrix;
- Expanding the number of participating mineral phases (in particular, zeolites).

2.1.3 Model developments under consideration

- Coupling of gas species partial pressure to total pressure;
- Improving activity coefficient calculation methods;
- Incorporating additional kinetic rate laws;
- Evaluating system conditions at final dryout and initial rewetting;
- Incorporating the MINC model for a refined mesh in the matrix blocks;
- Incorporating temperature and species-dependent diffusion coefficients for aqueous and gas phase species.

3. BACKGROUND AND PREVIOUS WORK

The quantity of water entering the Engineered Barrier System (EBS) and its chemical behavior are essential to understanding the performance of the EBS and the influence of coupled THC processes on the alteration of the natural system. Water entering the EBS has the potential for contacting waste packages. The chemical composition of the water (e.g., pH, dissolved solids), which will be modified by repository thermal processes, has a direct bearing on corrosion rates and processes, and therefore may impact waste package performance. Hot water also has the potential for altering fracture mineral coatings, for dissolving mineral constituents such as silica and calcite at near-boiling temperatures close to

the repository drifts, and for redepositing salts and mineral coatings in cooler regions farther away from the drifts. Potential changes in fracture coating mineralogy could change the transport properties of the rock over time. Circulating hot water could dissolve fracture mineral coatings in some areas and precipitate them in others, thus altering the permeability of the near-field environment. These rock-water interactions will operate over time scales far beyond our ability to monitor and observe them. However, data collected from *in situ* tests coupled with predictive models should advance our confidence in the ability to bound these processes.

3.1 Purpose of DST

The DST, which began on December 3, 1997 in the Exploratory Studies Facility (ESF), is designed to gain a better understanding of coupled thermal, hydrological, mechanical, and chemical processes likely to occur in the rock mass surrounding a potential repository at Yucca Mountain. Coupled processes in the DST will be monitored over an eight-year period as the test progresses through four years of heating, followed by four years of cooldown after the heaters are turned off. The DST has nine canister heaters, placed in a drift with a heated length of 47.6 m and flanked by 25 borehole wing heaters in each wall. The drift wall temperature will approach 200°C during the test (Birkholzer and Tsang, 1997). Sensors installed in over ninety instrumented boreholes monitor temperature, humidity, gas pressure, and mechanical displacement of the rock mass. Neutron logging, electrical resistivity tomography, cross-hole radar tomography, and air injection tests will be performed at intervals to measure moisture redistribution due to boiling, vaporization, and condensation of pore water. Liquid water and gas samples, collected opportunistically, will be analyzed to determine water-rock interaction. Passive monitoring and active testing data are intended to provide a base for modeling coupled thermal-hydrological-chemical processes, in order to advance understanding and reduce uncertainty in predicting repository performance.

3.2 THC regimes in the repository and in the DST

The evolution of the thermo hydrologic regime in the unsaturated zone surrounding the DST can be described in terms of processes occurring during the heating and cooling stages. During heating, THC reactions will occur in boiling and condensation zones. These are shown schematically for the potential repository at Yucca Mountain in Figure 3.1.

3.2.1 Boiling zone

During the initial heating stage, rocks will be heated significantly above the boiling point, and evaporation and boiling of pore waters will take place. Along with evaporation and boiling, other processes are expected to occur. These include: 1) saturation with respect to calcium

and magnesium sulfates and hydrated silicates; 2) transient dissolution of primary and some secondary minerals in response to a new equilibrium state imposed at elevated temperatures; 3) transient supersaturation and precipitation of secondary minerals resulting from the enhanced dissolution of primary minerals; 4) hydrolysis in response to elevated temperatures; and 5) partition of some volatiles and gases into the vapor phase, e.g., CO_2, HCl, N_2O, $B(HO)_3$ (and NH_4Cl).

3.2.2 Condensation zone

A condensation zone will occur beyond the volume of rock in which boiling takes place. Although the boiling point of water at Yucca Mountain is ~95°C, the condensation boundary temperature will be modified by capillary action and a lowered vapor pressure due to dissolved salts. Within the condensation zone, the following are expected to take place: 1) dilution of pore waters with condensate; 2) enhanced dissolution of primary and secondary minerals in response to the new equilibrium state imposed by elevated temperatures; 3) uptake of volatiles and gases from the vapor phase; 4) above the drift, drainage of the aqueous liquid towards the boiling front, followed by possible repeated evaporation of the aqueous phase and precipitation of transported solutes; 5) some secondary precipitation of silica at declining temperatures in places where the aqueous liquid drains toward cooler regions.

3.2.3 Cooling phase

The heated rock will begin to cool down after the heaters are turned off in the DST. During the cooling phase, the boiling front will retreat towards the drift walls. As the boiling front retreats, a coating of mineral precipitates will be deposited along fractures and perhaps to some degree into pores. Above the drift, the downward retreating front may induce redissolution of previously precipitated salts, and concentration of the salt load at the migrating front, that may lead eventually to fracture sealing.

Water that interacts with repository materials will be a mixture of fracture water, pore water, and condensate that has interacted with rock fracture mineralogy. Evaporative concentration will produce different effects, depending upon conditions such as CO_2 fugacity. During repository heating, evaporative processes will dominate and the water composition will depend on the extent of evaporation. Most of this water will be derived from ambient percolation but some may be refluxed condensate. During cool-down, the water composition will be dominated by condensate and the actual composition will depend on the extent of rock-water interaction. Water of this more evolved nature is most likely to interact with repository materials. At the edges of the repository and toward the end of the cooldown period, the water composition will be more similar to that of fracture flow waters.

3.3 Insights on THC behavior from tests and geothermal analogues

3.3.1 Laboratory tests

Batch studies of hydrothermal alteration of wafers of Topopah Spring Tuff, both welded and devitrified, have been performed at temperatures of 90°, 120° 150°, and 250°C for up to 120 days (Knauss, 1986; Knauss and Beiriger, 1984; Knauss et al. 1984, 1985, 1986, 1985a,b, and 1987; Knauss and Peifer, 1986; Oversby, 1984a,b, and 1985). These studies showed only minor changes in the composition of water in contact with the tuff at temperatures as great as 150°C, with slight alteration of the tuff over a few months. At higher temperatures reaction rates increased significantly. Accelerated experiments on crushed tuff at temperatures greater than 150°C produced the most extensive alteration, including the production of metastable phases. Knauss et al. (1984) found that at 150°C the dominant secondary phases produced by the experiment were mainly clays (gibbsite, illite, and Fe- and Mg-rich clay) and zeolites (mordenite and dachiardite), and at 250°C the dominant secondary mineral was dachiardite. SEM photographs indicated etch pits on feldspar and corrosion of biotite at these temperatures.

Laboratory experiments have also been conducted to study the alteration of zeolitized and vitric tuff. The upper and basal Topopah Spring vitrophyres contain reactive glass and secondary minerals, and these strata are potentially important to repository performance (although vitric and zeolitic horizons are not found in the ESF in areas of the heater tests). Knauss and Copenhaver (1995) reported an experiment that examined alteration of polished wafers of unaltered, densely welded Topopah Spring vitrophyre. At temperatures of 150°C and less, only glass dissolution was observed. In another experiment, Knauss and Copenhaver (1995) examined the alteration of naturally zeolitized samples from the same vitrophyre. These samples were stable to further alteration. From these experiments, it may be inferred that the reaction of water with glass will be slow at temperatures up to 150°C, compared to the experimental time scale.

Zeolites, due to their high water content, may have a significant effect on the heat and water balance in zones where they are abundant (Bish, 1995; Bish et al., 1996; Carey and Bish, 1996b). According to these studies, zeolite dehydration is reversible, such that rehydration will occur during cooldown. These studies indicated that dehydration of zeolites will cause some degree of shrinkage that increases porosity and permeability, and could affect the behavior of water perching at altered zones associated with the upper and lower Topopah Spring vitrophyres. Bish and Chipera (1994) showed that nearly two years of steam heating of zeolites did not alter them or transform them to other phases. They also reported in the same study that short-term heating of smectites to 150°C produces irreversible reduction in their swelling capacity.

Plug-flow reactor studies involving flow-through reaction of deionized water with Topopah Spring tuff at 240°C resulted in significant dissolution of alkali feldspar and cristobalite (DeLoach et al., 1997). The data from this experiment are significantly different from batch reactor studies at similar temperatures (as described above), in which alteration, rather than dissolution, predominated. Results of the plug-flow reactor experiments were simulated by Johnson et al. (1997a) using the reactive transport simulator GIMRT (Steefel and Yabusaki, 1996). Results of the plug-flow reactor experiments were also modeled using TOUGHREACT in this study, as described in section 9.0.

Numerous studies have been conducted to investigate variations in matrix permeability with temperature. These studies showed that within-sample permeability variations associated with temperature changes are less than variations between samples of Topopah Spring welded tuff at one temperature (Lin and Daily, 1984, 1988, 1989, 1991; Lin, 1990; Lin and Roberts, 1996; Moore et al., 1985; 1986; Morrow et al., 1984; Reda, 1985). Lin and Daily (1984) also investigated the permeability of the welded tuff matrix to steam and found it to be comparable to water permeability. Lin et al. (1997) investigated the effect of differential pressure on fracture healing and showed a permeability decrease with increasing pressure, but the greatest decrease in pressure amplitude occurred during the initial heating cycle. Lin et al. (1997) reported that in fractured samples, dissolution and deposition of calcite and silica on fracture surfaces due to flowing of hot water caused fracture healing, and that healing is insensitive to fracture surface conditions. Their ongoing experiments demonstrate that fracture permeability decreases with time, with a rapid drop in permeability at high temperatures (Lin et al., 1997).

3.3.2 Field tests

Field tests conducted at G-Tunnel, the Fran Ridge Large Block Test, and the ESF Single Heater Test have been designed to look primarily at thermohydrologic and thermomechanical coupling phenomena. The G-Tunnel and Single Heater Tests were strongly over-driven, in that heat fluxes were about five times higher than would be the maximum average heat flux for the repository. Even so, some of the observations and results of these tests are important to bear in mind for understanding the scale of coupled processes with respect to THC models. In the first heater tests at G-Tunnel, (Lin et al., 1991; Ramirez et al., 1989 and 1991), moisture redistribution was observed with boreholes spaced 0.5 m apart; the maximum radius of the dryout zone was determined to be about 0.7 m. Some shedding of condensate to the sides of the heater was observed, but no water accumulation was observed in any borehole. In the Single Heater Test (SHT) (Lin, 1997) moisture redistribution was observed on the scale of about a meter. The dryout zone was apparently more centered on the heater than it was in the G-Tunnel tests. During the SHT water was collected after 70 days and twice more during the 270-day period of heating.

Approximately 2000 L of water was boiled from the dryout zone, which had a maximum radius of about 0.9 m. Isotopic and inorganic chemical analyses of the water have been carried out.

Significant amounts of water have been mobilized as fracture flow in field-scale heater tests. In G-Tunnel, drying fronts proceeded along fractures during heating, and rewetting occurred near fractures during cooling. In the Fran Ridge Large Block Test, a reflux event lasting less than an hour involved a quantity of water sufficient to change the temperature of much of the block. Over such a short time period, this can only have occurred by fracture flow.

3.3.3 Geothermal analogues

Numerous geothermal systems possess some similarities to the hydrogeologic system at Yucca Mountain, but these have not been studied exhaustively from the perspective of coupled processes behavior and predictions for a Yucca Mountain repository. To gain a better understanding of water-rock interactions at the field-scale, the geothermal systems of the Taupo Volcanic Zone (TVZ) were modeled using geochemical codes such as EQ3/6 (Bruton et al., 1993a). TVZ silicic volcanic rocks are similar in composition to high-silica rhyolites at Yucca Mountain, and temperatures in accessible parts range from 25° to 300°C, producing a variety of secondary minerals similar to those anticipated to form under repository conditions at Yucca Mountain. Even though the TVZ is fully saturated, extensive regions of the rock mass fall in the temperature range of 20° to 100°C and effects of boiling are observed.

The EQ3/6 code package was tested at temperatures encountered in TVZ boreholes using analyses of solution compositions and mineral assemblages (Bruton et al., 1993a; 1994). An equilibrium approach was taken under the assumption that systems at temperatures greater than 200°C would be at equilibrium. In comparing mineral assemblages predicted for two geothermal wells with observed assemblages sampled by drilling, major phases such as quartz and calcite were calculated to be at near-equilibrium, whereas phases such as wairakite and epidote were not predicted as accurately. This discrepancy could have been due to kinetic considerations, inadequacy of thermodynamic data, boiling effects, model assumptions or other considerations.

Viani and Bruton (1992) took an equilibrium approach to modeling fluid-rock interaction at Yucca Mountain using the EQ3/6 code (Wolery, 1993; Wolery and Daveler, 1992) and interacted J-13 water with Topopah Spring welded, devitrified tuff. Their modeling indicated that the formation of secondary mineral assemblages at increasing temperatures would produce the same suite of minerals as found in diagenetic zones I and II (of Carlos et al.

1993) at Yucca Mountain. At 90°C the final simulated assemblage would consist of cristobalite, K-feldspar, dioctahedral smectite and muscovite (a proxy for illite/smectite).

An understanding of silica precipitation is important because geothermal systems commonly have an impermeable silica-rich rock that caps and sometimes surrounds the zone of convective fluid and heat flow. In the majority of geothermal systems, and in all vapor-dominated fields, such as The Geysers, the caprock is produced by self-sealing. This is most commonly attributed to the deposition of silica, but may also be due to hydrothermal formation of secondary mineral phases such as clays and zeolites, feldspars, calcite, pyrite, and hematite (Grindley and Browne, 1975). Silica deposition is likely to be greatest where the temperature decrease is most abrupt, particularly at the margins of the fields.

Rates of silica precipitation from thermal fluids have been analyzed and compared with laboratory-derived rate data (Carroll et al., 1995). Their comparison pointed to significant discrepancies between results obtained with different test conditions. Field measurements of amorphous silica precipitation rates were made in hydrothermal waters of the TVZ and were compared with rates measured in the laboratory using similar techniques (Carroll et al., 1996). Precipitation rates on the order of 3×10^{-7} mol/m^2-day were obtained in the laboratory, which is within an order of magnitude reported by Rimstidt and Barnes (1980). Carroll et al. (1995) obtained similar results at buffered pH values of 3, 5, and 6 with slower precipitation at lower pH. Their results compared favorably with the pH dependence observed by Knauss and Wolery (1988). Carroll et al. (1995) also found that precipitation was more rapid in the presence of amorphous silica.

Precipitation rates measured in the field were 400 times faster than those obtained in laboratory experiments. Carroll et al. (1995; 1996) attributed this to several possible causes, including: 1) difference in solid phases between field (quartz) and laboratory tests (amorphous silica); 2) possible differences in effective surface area available for precipitation; 3) differences between closed-system transient adjustments in the laboratory experiments, and open-system steady-state processes in the field.

3.4 Insights from previous modeling studies

A plethora of simulations has been conducted over the past decade to attempt to quantify and bound coupled processes in the near-field environment and in the altered zone, which will extend tens of meters into the rock mass at different times over the period of repository heating and cooling. The simulations of coupled processes have been synthesized by Wilder (1996), Hardin and Chesnut (1997), and Hardin (1998). Two early simulations considered changes in water composition and changes in porosity due to THC processes. Glassley and Boyd (1994a) used the code FEHM and a 2-D, equivalent continuum approach to estimate

the rates and magnitudes of changes in THC properties. His results showed a 2% change in porosity, measured in the change in moles of silica in the rock. The porosity change translated to a three-order of magnitude change in permeability. Steady state was achieved in a few thousand years for most mineral reactions involving aqueous fluids. Deposition of silica occurred near the repository, with dissolution farther away. In another study, Glassley and Boyd (1994b) simulated near-field water compositional changes due to evaporation, as contrasted to boiling. When the gas composition was not controlled, solution pH was near neutral and Eh was slightly oxidizing. As H_2O activity decreased, Na, S, Cl, and F increased in the solution. SiO_2 was controlled by the solubility of quartz and chalcedony. When the gas composition was fixed at atmospheric O_2 and CO_2, pH increased to 9.0 and Eh became reducing at higher temperatures. A follow-up study (Glassley, 1997a) modeled the chemical composition of waters up to 150°C before contacting repository materials and in the absence of evaporation. In this study, calcite, quartz, and cristobalite became supersaturated in water that was in equilibrium with atmospheric CO_2. Factors controlling mineral saturation were the extent to which equilibrium with atmospheric CO_2 was achieved, and the extent to which supersaturation of silica polymorphs occurred before they precipitated. The simulated waters became more dilute than J-13 water, due to the effect of mineral precipitation on solution chemistry. Porosity changes on the order of 3-4% occurred at inlet and outlet points in the model, as cristobalite, calcite, and smectite continued to dissolve while hematite, K-feldspar, and Ca-clinoptilolite formed.

Some of the simulations that may be instructive to comparisons in this report were conducted with specifications of the DST. In one study, Glassley (1997b) examined the THC alteration of flow pathways above and below the repository. Results of his simulations showed that most mineral reactions occurred over the first fifty years. For the mineral phases considered, dissolution rates were 10^{-10} to 10^{-11} mol/cm^2/yr. This study furthermore predicted the following: 1) calcite dissolution would take place only where condensate forms, and is a strong function of fluid velocity; 2) amorphous silica dissolution is less below the drift than above it, and is not a function of fluid velocity; and 3) quartz and albite remained near saturation throughout. A second study (Glassley, 1997d) used the NUFT code and the GIMRT code to perform 2-D reactive transport predictions of the DST over a four-year period. For temperatures above 100°C, mineral changes were dominated by dehydration or alteration of existing vapor-phase minerals. From 40° to 100°C a large variation in chemistry took place, with strong compositional zoning reflecting the effect of flow length path on reaction progress (i.e., the shorter the flow path, the more dilute the solution). Glassley (1997d) noted that models of condensate development in fractures indicated the time-dependence of secondary mineral development and the spatial distribution of minerals. He concluded that the spatial distribution of precipitates is strongly sensitive to condensate flux and the spatial distribution of dissolution is only moderately sensitive to condensate flux.

Four THC modeling studies were presented by Hardin (1998) in his report of near-field models. The first was a reaction-path study using EQ3/6 for evolution of water in contact with the host rock. This study examined the uncertainty in reaction rate constants for water-rock interaction. Results showed that evolution of recharge water to the composition of J-13 depends principally on the rate of silica dissolution, but also on other rates of reaction, all of which are uncertain.

The second study simulated reactive transport of silica at the repository scale using FEHM. Changes in fracture porosity were coupled with permeability changes. Calculations showed that quantities of silica could be mobilized by repository TH processes to cause significant changes in local fracture porosity. Boiling occurred predominantly at the bottom of the isothermal heat pipe zone, where residual solids accumulated.

A third THC modeling study reported by Hardin (1998) involved fully coupled drift-scale THC calculations using the NUFT code with a dual permeability (DKM) formulation, which was modified to incorporate the behavior of silica. The model included coupled porosity and permeability and produced coupling between porosity and water potential and relative permeability curves. Reaction rates and chemical equilibria were temperature dependent. Chemical dissolution/precipitation reactions were modeled in both the fracture and matrix continua. The model predicted formation of a precipitation cap above emplacement drifts for all conditions considered, including ranges of the specific surface area available for silica dissolution, and reaction constants corresponding to different silica phases. The model showed that significant precipitate accumulated within a few years or tens of years after the start of heating. The model incorporated a lower bound on permeability reduction in the boiling zone to reflect the relationship between permeability and heat pipe formation, which showed upward migration of the zone of permeability reduction with time.

The fourth THC modeling study reported by Hardin (1998) performed coupled reactive transport simulations with the OS3D/GIMRT code (Steefel and Yabusaki, 1996). The simulations focused only on fracture flow conditions. The objective of these simulations was to examine implications of the more certain aspects of chemical behavior, while acknowledging substantial uncertainty in rate constants for silica dissolution and precipitation reactions, as well as fracture mineral inventory. The simulations showed that dissolution of calcite would occur rapidly, whereas aqueous dissolution and precipitation reactions involving silicates would produce more significant changes in porosity, but over longer time periods, on the order of tens of years. Later in the thermal evolution of the repository, CO_2 would be displaced from the gas phase by water vapor as the air mass fraction approaches zero in the host rock. OS3D/GIMRT simulations showed that decreased CO_2 fugacity would have little impact on calcite and silica reactions at near-neutral pH. The presence of condensate that is less chemically aggressive to calcite would result in the physical spreading of precipitation

and dissolution zones. The aqueous dissolution and boiling processes predicted by NUFT and by OS3D/GIMRT were shown to be incompatible above the emplacement drifts. Hardin (1998) stated the need for a model that would accommodate a full set of chemical reactions with evaporation, boiling and gas phase transport.

3.5 Mineralogy of the fractured tuff

The Topopah Spring Tuff is relatively homogeneous from the chemical viewpoint, but varies in the relative abundances of silica polymorphs (quartz, cristobalite, and tridymite) (Bish et al., 1996). Within the repository horizon, which extends from below the zone of abundant (15%) lithophysae to the basal vitrophyre of the Topopah Spring Tuff, more than 98% of the mineral content of the bulk rock is comprised of tridymite, cristobalite, quartz, and alkali feldspar (Bish et al., 1996). The abundance of feldspar varies from 55 to 65%. Hematite and smectite are common minor phases. The clay minerals at Yucca Mountain are predominantly interstratified illite/smectites (Bish, 1989) and are present in amounts from 1 to 10% in virtually every stratigraphic unit. The alkali feldspar (sanidine) compositions range from Or_{38} to Or_{66} (Broxton et al., 1989) with most in the range of Or_{45} to Or_{55}. Plagioclase compositions range from An_{14} to An_{20} with a minor compositional mode at An_{35} (Broxton et al., 1989).

Carlos et al. (1991, 1995) reported on fracture mineralogy taken from drill core in the lower Topopah Spring Tuff above the basal vitrophyre. They noted three generations of fracture sets. The first generation fracture set was connected to (and related to) lithophysae and was sealed by tridymite that may or may not have transformed to cristobalite or quartz. This set was surrounded by a bleached zone. Another fracture set contained crusts of mordenite over Mn-oxides, predominantly lithiophorite (Al- and Li-bearing) and rancieite (Ca- and Mg-bearing), with some todorokite (Na-, Ca-, and K-bearing). Both of these fracture sets are nearly planar and are often slickensided, and were interpreted by Carlos et al. (1991, 1995) to be more than 11.5 Ma in age. A later fracture set that post-dated tectonic activity was sequentially lined by the zeolites stellerite and heulandite, smectite, and finally calcite. Glassley (1997c) noted that fracture mineralogy is consistent at the horizon of the DST with calcite (89%), alkali feldspar (0.2%), amorphous silica (5%), quartz (5%), and clay (0.1%). He used these relative abundances in predictive models.

Petrographic studies of the Topopah Spring Tuff in the area of the DST (this study) show it to be moderately to densely welded, devitrified, and vapor-phase altered. Phenocrysts make up less than 2% of the sample and on an average there are fewer than 2% voids. The dominant phenocrysts are sanidine and plagioclase, with lesser biotite, quartz, and Fe-oxides. Accessory minerals include zircon and apatite. The bulk of the groundmass consists of devitrification products, alkali feldspar, quartz, and cristobalite. The percentages of these

were quantified by Roberts and Viani (1997a, b, see sect. 12.3). In some areas coarse granophyric crystallization has produced interlocking quartz and alkali feldspar. Relict glass shards and relict pumice are recognized in outline by nearly opaque clay and opaque oxide rims. Other relict vitric textures include spherulitic patches of silica, a feathery, fluid-looking groundmass, and a scalloped pattern of fine-grained, radial, fibrous quartz and/or alkali feldspar. These patterns are often nucleated on the surfaces of phenocrysts and relict pumice. Within lithophysal cavities, minute acicular crystals of quartz and alkali feldspar radiate from the walls. Vapor-phase crystallization includes quartz, quartz after tridymite, and alkali feldspar growing into void space.

Roberts and Viani (1997a,b) found that the abundances of quartz and cristobalite were inversely correlated. Tridymite and smectite were found in about 25% of the samples and clinoptilolite appeared in one sample. Fracture filling material observed included quartz, minor feldspar, calcite, hematite, manganese oxides, smectite, and a trace of tridymite. We recently obtained thin sections of samples taken from these locations and have identified a zeolite lining fractures as well (Simmons and Glassley, 1998). Roberts and Viani (1997a,b) noted that grayish alteration areas in the matrix contained a greater percentage of quartz and tridymite and lesser amounts of cristobalite than in the unaltered matrix. This is the opposite to x-ray diffraction patterns of Glassley and Boyd (1995) in which cristobalite dominated over quartz in bleached zones surrounding many fractures of the first generation. Additional mineralogic studies of samples from the DST and the SHT are underway that may shed light on this contradiction (this study and at Los Alamos National Laboratory).

4. QA STATUS OF CODES AND DATA

4.1 QA Status of Data Used in Report

The data used as input to modeling in this report come from a variety of qualified and unqualified sources, making data developed from these sources and conclusions derived from these data non-Q. The QA status of specific input data sources is provided in Table 4.1. The data fall into several classes and the mixed nature of their qualification status can easily be seen:

1. Mineralogy – these data come primarily from non-Q borehole studies or from experimental data collected prior to the Yucca Mountain QA program, e.g. Delany et al., 1986. The exception is x-ray diffraction mineralogy of the DST (Roberts and Viani, 1997a, b; see Table 4.1). Mineralogy data collected from petrographic analyses in this study are preliminary but will be qualified in FY98.

2. Thermodynamic data are taken from the EQ3/6 data base (Wolery, 1992), which consist mostly of data from SUPCRT92 (Johnson et al., 1992) and from Pokrovskii and Helgeson (1995), Holland and Powell (1990); and from SOLTHERM.HP and SOLTHERM.JOH data bases (same data sources, courtesy of M.H. Reed, University of Oregon). All of these are unqualified data sources.

3. Water chemistry data and strontium isotopic compositions come from both qualified and unqualified sources and are shown in Table 4.1.

4. Gas chemistry data is taken from Conrad (1998), unqualified.

5. Hydrologic parameters and other specifications of the DST are taken from Birkholzer and Tsang (1997), which used qualified DST design parameters and hydrologic properties taken from the UZ Site-Scale Model (Bandurraga and Bodvarsson, 1997). The latter uses both qualified and unqualified data.

6. Kinetic data are unqualified (from Johnson et al., 1996; Hardin, 1998; Rimstidt and Barnes, 1980).

The data developed as a result of new thermodynamic determinations are considered preliminary. The recalibration of pore water chemistry data is also preliminary and requires additional quality assurance checks. All of the model output data are considered scoping.

Table 4.1. Study Data Summary and Q Status

Borehole/Data Type Organization- Principal Investigator	Q Status	DTN/AN (if available)
XRD Mineralogy, LLNL, Roberts and Viani (1997a, b)	Y	DTN LL980106404244.050
J-13 well water, Various, Harrar et al., (1990)	N	Not available
G-1, G-3, G-4, UE25b-1H mineralogy LANL, Bish, Carlos, Broxton, various studies	N N N N	DTN LA000000000040.001 DTN LA000000000112.002 DTN LA000000000113.002 DTN LA000000000039.001
UZ Pore Water, USGS, Yang et al., 1996a	Q	DTN GS970108312271.001
Sr isotope data, USGS, Neymark et al., 1995	N	DTN GS941208319211.005
Sr isotope data, USGS, Paces et al., 1998	Q	DTN GS980308315215.009
		NA= Not Available; Y= qualified, N= unqualified data; TBQ = To be qualified

4.2 QA Status of Codes

TOUGH2 version 1.11 (Pruess, 1991), the flow module of TOUGHREACT, has been tested extensively and has met the requirements for Software Qualification defined in LBNL Quality Implementing Procedure YMP-LBNL-QIP-SI.0 (Pruess et al., 1996; Wu et al., 1996). The qualification of TOUGHREACT is currently underway and the code cannot be considered QA at this time. Nevertheless, several benchmark tests have been performed as part of this study to verify the overall behavior of the geochemical reaction and transport modules of TOUGHREACT (Section 9.0). It is our intent to incorporate the results of these tests into software qualification of TOUGHREACT for the Yucca Mountain Project. In addition, reactive transport at 25°C has been extensively verified against analytical solutions and other simulations for a wide range of processes (Xu et al., 1998a, b; Xu, 1996).

Although EQ3/6 v.7.2b is qualified for use in the Yucca Mountain Project, neither SUPCRT92, nor the thermodynamic data embodied in SUPCRT92 have been qualified. The integrity of the data therefore depends on the traditional process of peer review and scientific testing. CHILLER (Reed, 1982; Spycher and Reed, 1992) has not been qualified for use on the Yucca Mountain Project, although it has been applied in the past to modeling boiling of

pore waters at Yucca Mountain (Reed, 1988). It has been tested extensively for modeling gas-water-rock interactions for the geothermal, mining, and oil industries. We do not intend to qualify it under Yucca Mountain Project software QA procedures.

5. CONCEPTUAL MODEL OF THERMO-HYDRO-CHEMICAL PROCESSES FOR THE DST

Different geochemical processes will take place in fractures and in the matrix, depending on the flow of water, water vapor, and heat in fractured tuff. There are several reasons for this. First, the fracture mineralogy is significantly different from that in the matrix, with common secondary mineralization of predominantly calcite, opal, clays, and zeolites (Paces et al., 1998). There is little secondary mineralization in the low permeability welded tuff matrix. Second, aqueous and gas phase transport by advection in open fractures can be orders of magnitude greater than in the matrix. Third, physical processes caused by heating of the unsaturated rock lead to more rapid dryout in fractures in the dryout region and strong condensation effects in fractures over a large region (Buscheck et al., 1997a,c). These effects can lead to large differences in the chemical compositions of fluids in fractures and adjacent matrix blocks.

Thus, it is foremost that we begin our conceptual model of the THC system with a good approximation of the physical aspects of the system. The dual permeability model has been shown to provide much better agreement than the equivalent continuum model (ECM) to the thermal and saturation results of the Single Heater Test (Birkholzer and Tsang, 1996, 1997). As a conceptualization of the primary mineralogical differences in the welded tuff, dual permeability allows the mineralogical aspects to be specific to fractures and matrix separately, with geochemical communication through imbibition and diffusion (Figure 5.1). There are also significant drawbacks to the dual-permeability concept, as it represents chemical diffusion between matrix and fracture continua as a flux associated with a linear concentration gradient. The choice of how liquid saturations are averaged at matrix-fracture interfaces can dramatically change the calculated diffusive chemical fluxes. The results of our testing have shown that this is exacerbated by the more rapid loss of water in fractures undergoing dryout as compared to the matrix.

Another consideration that is peculiar to the thermal tests and near-field of the repository is the transition over time to complete dryout of the region adjacent to the thermal source. Water-rock interaction models need an aqueous phase to be present in the simulated system to allow computations of reactions between water and rock. In addition, treating evaporation of the last remaining water (residual saturation) is not straightforward because there are limits

to the applicability of such models at high ionic strengths. For the current conceptualization of the thermal test regime, we consider that the most important mineralization and geochemical effects are those that occur above a certain liquid saturation level. For the simulations presented here, we assume that all geochemical interactions, and diffusive and advective chemical fluxes are zero below a liquid saturation of 1×10^{-5} (for one case, 1×10^{-4}). At this point we save the final water chemistry so that under conditions of rewetting incoming fluids will mix with this residual fluid. This approximates the instant precipitation and dissolution of highly soluble salts at low water contents without being forced to calculate their actual identity under these extreme conditions.

The conceptualization of reacting minerals is that they are present in given amounts (from mineralogical studies or estimated) and that they are characterized by an unchanging reactive surface area. Assuming that the initial characterization of the reactive surface minerals in the system (effective relative to the rock texture, pore structure, etc.) is correct, which is unlikely, the surface areas available for reaction will certainly change over time. This will occur not only through dissolution and precipitation producing different amounts of the minerals, but also through coating of mineral grains by other mineral precipitates, resulting in areas that are unavailable to the pore fluid, except possibly through grain boundary diffusion or diffusion through mineral coatings (Sonnenthal and Ortoleva, 1994). Because the latter processes are diffusion-limited, they are likely to be effective only over much longer time-scales than for direct pore fluid-mineral reactions.

Rates of reactions and mineral assemblages are highly dependent on the pH, which for the conditions associated with the Drift-Scale thermal test is a strong function of the partial pressure of CO_2 in the gas phase, as well as of the mineral-water reactions. A realistic model of the geochemical conditions of fluids and mineral alteration phenomena must consider interactions with CO_2 in the gas phase, as well as typical water-rock interaction effects. Given this consideration, our conceptual model starts with the incorporation of gas species transport and CO_2 equilibria between liquid and gaseous phases. This added realism, though, makes the solution of the reaction-transport problem much more difficult. Diffusion in the gas phase and gas flow velocities are much higher than that for aqueous species and fluid transport. Thus, there are significant numerical limitations, primarily in the time step size. Coupling the CO_2 transport to mineral/water reactions also causes much more nonlinearity in the system as phases are affected by rapid flow velocities and the strong temperature dependence of CO_2 partial pressure, which itself drastically affects pH. For these reasons, and the introduction of dual permeability concepts, the modeling we present here does not cover all of the minerals and aqueous species we may want to consider; however, we believe that the basis for this work will lead to a much better long-term analysis.

6. DEVELOPMENT AND ANALYSIS OF THERMODYNAMIC DATA FOR THE DST

6.1 Revision of Thermodynamic Data

Thermodynamic data of participating phases and aqueous species in natural systems are derived from a variety of sources, including low and high temperature heat capacity measurements, heats of solution data, using either lead borate or hydrofluoric acid, high temperature/pressure phase equilibria, and solubility data. Numerous internally consistent thermodynamic databases of naturally occurring minerals have been compiled from these disparate sources in recent years (e.g. Berman 1988; Holland and Powell 1985, 1990; Powell and Holland 1990; Gottschalk 1997), and they have been used extensively for geochemical modeling.

Thermodynamic data for aqueous species are similarly drawn from a variety of experimental methods including the use of electrochemical cells, calorimetric procedures and solubility studies. Major uncertainties remain from attempts to represent the thermodynamic data of aqueous species under standard state conditions, which require the application of suitable electrolyte models. Furthermore, not all species germane to the problem at hand have necessarily been identified, and their omission can result in cumulative systematic errors in reactive chemical transport models.

The EQ3/6 thermodynamic database, which is used as a basic source for this study, consists of the solubility products and dissociation constants of solid phases and aqueous species respectively, calculated at discrete temperature increments along the saturation surface for the aqueous phase between 0 and 300°C. A significant proportion of these data have been calculated using thermodynamic equations derived by Helgeson and his coworkers (Helgeson and Kirkham 1974a, b, 1976; Helgeson et al., 1978) in the SUPCRT92 code (Johnson et al., 1992). The latter code contains thermodynamic data for solid phases derived from a relatively early thermodynamic compilation by Helgeson et al. (1978) with subsequent corrections. Thermodynamic data for aqueous species in SUPCRT92 are presented in terms of the Helgeson, Kirkham, and Flowers (HKF) equation of state parameters, the parameters having been drawn from a series of papers by Helgeson and his co-workers (Helgeson et al., 1981; Shock and Helgeson, 1988, 1990; Shock et al., 1989; Sverjensky et al., 1997; Shock et al., 1997).

Since the publication of Helgeson et al. (1978), a number of new experimental studies have been reported, which mandate a revision of some of the thermodynamic data. The findings of some of these studies have already been incorporated, e.g. Pokrovskii and Helgeson (1995). But others of particular relevance to phase relations at Yucca Mountain have not.

The most important of these include a study of the low temperature aqueous solubility of quartz by Rimstidt (1997), revised thermodynamic data for coexisting illite and smectite (I/S) by Aja (1995) and Kulik and Aja (1997), solubility measurements of sepiolite and kerolite by Stoessell (1988), and a revised correlation of the thermodynamic properties of low albite and potash feldspar, based on field data of the $[Na^+]/[K^+]$ ratio (Apps and Chang, 1992).

Fortunately, only a restricted subset of phases must be considered, and their thermodynamic properties accurately determined to model effectively the thermochemical environment of the DST in the Tptpmn Unit. In addition, all significant aqueous species must be included. The preliminary assessment of pore water compositions and potential thermodynamic controls (Section 7) indicates, however, that at a minimum, the following phases must be included:

- Low albite
- K-feldspar (microcline)
- I/S phases, i.e. illite and smectite
- Kaolinite
- Sepiolite
- Calcite
- Quartz
- Cristobalite
- Amorphous silica, i.e. opal-A

Several other phases could be important, but further evaluation will be necessary, either to refine their solubility products as a function of temperature, or to establish whether they are likely to be significant participants in thermochemical processes in either the DST or the proposed repository. They include several zeolites, particularly heulandite, stellerite, and mordenite as well as poorly defined amorphous alumino-silicates and opal-CT. Zeolites are in general infrequently observed in the matrix, but have been noted somewhat more commonly in fractures in the devitrified units and this might be attributed to devitrification of the tuff to a mineral assemblage that is as stable or possibly more stable than the cited zeolites. Investigations are underway to clarify this issue.

One of the most important areas of concern in revising the ESQ3/6 database (DATA0) is the erroneous determination of the thermodynamic properties of $SiO_2(aq)$ by Walther and Helgeson (1977). In their study, they rejected two consistent data sets by van Lier et al. (1960) between 60 and 100°C, and Siever (1962) between 125 and 180°C in favor of

incompatible data by Morey et al. (1962) and Mackenzie and Gees (1971) at 25°C. This interpretation contrasted with that by Apps (1970), who considered the datasets by Van Lier et al. and Siever to be valid (see Figure 6.1). Subsequently, Rimstidt (1997) conducted a careful study of quartz solubility between 25 and 95°C and obtained results that were consistent with Van Lier et al. and Siever. Rimstidt's interpretation is also substantiated by consistency between the thermodynamic properties of SiO_2(aq) obtained from amorphous silica solubility. Walther and Helgeson (1997) calculated the HKF equation of state parameters for SiO_2(aq) from a regression of selected solubility measurements, and these parameters were included in the SUPCRT92 database from which solubility products for many silicates and aluminosilicates in DATA0 were derived. Time constraints prohibit a redetermination of the HKF parameters for SiO_2(aq) at this time. Instead a more pragmatic approach was taken in revising the solubility products of the phases listed above. These revisions, while not entirely consistent internally, are sufficiently accurate for preliminary model simulations of the DST. Any subsequent refinements will lead to minor differences that will have no quantitative significance.

The nature of the revision depends on the original source of the Gibbs free energy of formation, $\Delta G^\circ_{f\,298.15}$ of the solid phase at the reference temperature and pressure, i.e., at one atmosphere (10^5 Pa) and 298.15 K. For those phases where $\Delta G^\circ_{f\,298.15}$ was derived from aqueous solution measurements, a revision is undertaken by consulting the original source material. For those solid phases where $\Delta G^\circ_{f\,298.15}$ is based on calorimetric determinations, the solubility products must be recomputed using revised quartz solubility data. For the phases listed above, the following procedures were adopted to determine their solubility products at 0, 25, 60, 100 and 150°C.

6.1.1 Low Albite

The recommended value for low albite from Berman (1988) was adopted, and the following equations used to compute the solubility products:

$$\underset{\text{low albite}}{NaAlSi_3O_8} = Na^+ + AlO_2^- + 3\underset{\text{quartz}}{SiO_2} \qquad (6.1)$$

$$\underset{\text{quartz}}{SiO_2} = SiO_2(aq) \qquad (6.2)$$

Solubility products for the first equation were computed using SUPCRT92 with data from a modified (Johnson et al., 1992) database. Solubility products for the second equation were computed from the solubility equation for quartz given by Rimstidt (1997). The solubility products from both equations were added to obtain the solubility products for the equation:

$$\underset{\text{low albite}}{NaAlSi_3O_8} = Na^+ + AlO_2^- + 3\,SiO_2(aq) \qquad (6.3)$$

6.1.2 Potash Feldspar

The same procedure as for low albite was adopted, using a corrected $\Delta G^{\circ}_{f\,298.15}$ value for potash feldspar from Apps and Chang (1992).

6.1.3 I/S Phases: Illite

$\Delta G^{\circ}_{f\,298.15}$ and $S^{\circ}_{298.15}$ for illite with the formula $K_{0.5}(Mg_{0.22}Al_{1.78})(Al_{0.28}Si_{3.72})O_{10}(OH)_2$ was corrected from values provided by Kulik and Aja (1997) using the following phase equilibrium relation determined experimentally by Aja (1995) at temperatures between 25 and 250°C:

$$K_{0.5}(Mg_{0.22}Al_{1.78})(Al_{0.28}Si_{3.72})O_{10}(OH)_2 + 0.94H^+ + 0.59H_2O = 0.5K^+ + 0.22Mg^{2+}$$
illite
$$+1.66SiO_2(aq) + 1.03\ Al_2(SiO_2)(OH)_4 \qquad (6.4)$$
kaolinite

using the thermodynamic properties for kaolinite from Robie and Hemingway (1995), and the thermodynamic properties for $SiO_2(aq)$ computed from the data for H_4SiO_4 by Rimstidt (1997). The revised values were entered in the SPRONS96.DAT database of SUPCRT92 together with molar volume and heat capacity data reported by Kulik and Aja (1997), and the solubility products calculated for the reaction:

$$K_{0.5}(Mg_{0.22}Al_{1.78})(Al_{0.28}Si_{3.72})O_{10}(OH)_2 = 0.5K^+ + 0.22Mg^{2+} + 2.06AlO_2^-$$
illite
$$+3.72SiO_2(aq) + 1.12H^+ + 0.44H_2O \qquad (6.5)$$

6.1.4 I/S Phases: K-Smectite

$\Delta G^{\circ}_{f\,298.15}$ and $S^{\circ}_{298.15}$ for K-smectite with the formula $K_{0.29}(Mg_{0.26}\,Al_{1.74})(Al_{0.03}Si_{3.97})O_{10}(OH)_2$ was computed in a similar manner to that of illite, and from the same literature sources cited for illite, and the solubility products calculated for the reaction:

$$K_{0.29}(Mg_{0.26}\,Al_{1.74})(Al_{0.03}Si_{3.97})O_{10}(OH)_2 = 0.29K^+ + 0.26Mg^{2+} + 1.77AlO_2^-$$
k-smectite
$$+3.97SiO_2(aq) + 0.96H^+ + 0.52H_2O \qquad (6.6)$$

6.1.5 I/S Phases: Ca-, Mg-, Na- Smectites

Solubility products for Ca-, Mg- and Na- smectites were calculated from those reported for "Montmor-K", "Montmor-Ca", "Montmor-Mg", and "Montmor-Na" in the DATA0.COM

database of EQ3/6 v.7.2b by referencing K-smectite to "Montmor-K", and correcting the solubility constants for the remaining smectites after adjusting for minor differences in stoichiometry between the K-smectite cited above, and the montmorillonites reported in DATA0.COM, i.e. $K_{0.33}Mg_{0.33}Al_{1.67}Si_4O_{10}(OH)_2$, etc. For modeling purposes, these end member smectites serve to represent the contributions of each respective cation in the interlayer exchange positions of the smectite component of I/S. Ideally, a solid solution model should be incorporated in the model to describe the interlayer cation occupancy, and this will be done when time permits.

6.1.6 Kaolinite

In order to insure consistency with the I/S phase solubility products, the thermodynamic properties for kaolinite reported by Robie and Hemingway (1995) were entered in SPRONS96.DAT of SUPCRT92, and the solubility products computed by summing the computed solubility products from the following two equations:

$$Al_2Si_2O_5(OH)_4 = 2AlO_2^- + 2H^+ + 2SiO_2 + H_2O \quad (6.7)$$

kaolinite quartz

$$SiO_2 = SiO_2(aq) \quad (6.8)$$

quartz

where the solubility equation for quartz is given by Rimstidt (1997), to give the solubility products for the reaction:

$$Al_2Si_2O_5(OH)_4 = 2AlO_2^- + 2H^+ + 2SiO_2(aq) + H_2O \quad (6.9)$$

Kaolinite

6.1.7 Sepiolite

The solubility products for the reaction:

$$Mg_2Si_3O_{7.5}(OH)\cdot 3H_2O + 4H^+ = 2Mg^{2+} + 3SiO_2(aq) + 5.5H_2O \quad (6.10)$$

sepiolite

were calculated directly from the reported values by Stoessell (1988).

6.1.8 Quartz

Solubility products for quartz were calculated from the solubility equation for quartz reported by Rimstidt (1997).

6.1.9 Cristobalite

The solubility products for cristobalite were calculated from:

$$\text{Log}K_s(\text{cristobalite}) = -970.05/T - 0.0787 \qquad (6.11)$$

This equation is based on a regression by Apps (1970) of pressure-corrected cristobalite solubility data derived from measurements by Fournier and Rowe (1962).

6.1.10 Amorphous Silica

The solubility products for amorphous silica were calculated from:

$$\text{Log}K_s(SiO_{2(am)}) = -679.19/T - 0.3848 \qquad (6.12)$$

This equation is based on regression by Apps (1970) of amorphous silica solubilities from a number of sources in the literature, as shown in Figure 6.2. The consistency of these data sets strongly suggests that this metastable form of silica may be a synthetic equivalent of opal-A. The precipitation of amorphous silica is most likely to occur during evaporation of condensate during the DST, and is therefore an essential phase in thermochemical modeling simulations of the DST.

A summary of solubility products of the phases identified for incorporation in the model is given in Table 6.1.

Table 6.1 Solubility products for the phases modeled in the DST (for reactions as shown in text).

	Temperature, °C				
	0	**25**	**60**	**100**	**150**
Low Albite	-21.694	-20.177	-18.362	-16.684	-15.094
Microcline	-24.861	-22.910	-20.619	-18.526	-16.549
Kaolinite	-43.073	-39.895	-36.336	-33.181	-30.212
K-Smectite	-43.004	-39.829	-36.275	-33.110	-30.093
Ca-Smectite	-42.523	-39.519	-36.156	-33.159	-30.303
Na-Smectite	-42.628	-39.528	-36.049	-32.937	-29.956
Mg-Smectite	-42.583	-39.613	-36.049	-32.937	-29.956
Illite	-45.354	-41.926	-38.294	-34.994	-31.867
Quartz	-4.079	-3.739	-3.349	-2.992	-2.642
α-Cristobalite	-3.630	-3.332	-2.990	-2.678	-2.371
Amor. Silica	-2.871	-2.663	-2.423	-2.205	-1.990
Sepiolite	17.28	15.76	13.83	12.08	10.45

7. WATER AND GAS CHEMISTRY

7.1 Water Chemistry

7.1.1 Statement of the Problem

The hydrochemical response of the DST must be modeled using a thermodynamic and kinetic database that has been calibrated against the pre-existing ambient hydrochemistry of the vadose zone at Yucca Mountain, and in particular, the Tptpmn Unit. Calibration is needed because extant thermodynamic and kinetic databases have been derived independently for conditions that do not necessarily match those at Yucca Mountain. Such conditions as phase metastability, surface free energy contributions, solid solutions, ion exchange, and adsorption may all affect the degree of correlation between theoretical prediction and field observation. Furthermore, despite extensive experimental investigations over several decades, thermodynamic data for some aqueous species and solid phases are still imprecise, incomplete or unknown. Furthermore, uncertainties in much of the thermodynamic data exceed by far, the degree of accuracy required for predictive modeling of the DST (e.g. see Apps and Chang, 1992). Hence the need for calibration, provided that the calibration process does not violate the uncertainties inherent in extant thermochemical data.

An analysis of pore water chemistry at Yucca Mountain is presently under way, using the species distribution code EQ3, v7.2b which forms part of the EQ3/6 package (Wolery, 1992).

An earlier investigation of the chemical composition of the pore waters recovered from drill core from UZ-14 at Yucca Mountain (Apps, 1997) suggested that the pore waters may have achieved local equilibrium with respect to primary and secondary minerals of the host rocks. This assumption was based on the relative invariance of log activity ratios representing the primary rock-forming oxide components. The analysis was based on an assumption that calcite was at or near saturation throughout the vadose zone. However, the analysis was of just one data set of several collected by Yang et al. (1988, 1996a,b) from drill holes NRG6, NRG7a, SD-7, SD-9, SD-12, UZ-4 and UZ-16, and perched waters collected from several of the holes (Yang et al., 1996a). Because a larger number of samples would establish the degree of variability in pore water compositions at Yucca Mountain, and would assist in refining and calibrating the thermodynamic controls on pore water composition, the analysis was extended to include all available data. The analysis consists of two steps: (1) an evaluation of the consistency and quality of the chemical analysis, and (2) a preliminary interpretation of pore water equilibrium with respect to primary and secondary minerals.

7.1.2 Evaluation of Pore Water Analyses for Consistency

A number of tests can be performed to check the consistency and validity of chemical analyses. These checks are a necessary requirement before a thermodynamic evaluation can be performed. The following checks were performed on all chemical analyses reported by Yang (1992) and Yang et al. (1996a,b and corrections).

- Augmentation of the analyses by the addition of K^+ at a concentration of 4.0 mg/L. In Yang's analyses, K^+ was not reported for all but seven pore water analyses. Perched waters and those pore waters analyzed for K^+, showed a range from 4 to 16 mg/L. However, waters sampled below 100 m depth were usually toward the low end of the range.

- Omission of Al analyses. Those Al analyses reported were unrealistically high for pore waters, and appear to represent artifacts of the analytical procedure, representing the dissolution of suspended particulates by nitric acid.

- Correlation of SiO_2(aq) analyses for contamination introduced by the dissolution of clay particulates. These were corrected using a correlation plot, as illustrated in Figure 7.1, except for several anomalous values reported for pore water from UZ-14.

- The assumption that total HCO_3^- (in mg/L) is equal to the sum of HCO_3^- + (61/60)CO_3^{2-}. Alkalinity titrations are reported in terms of CO_3^{2-} above pH = 8.3, and HCO_3^- between pH = 8.3 and pH = 4.5. Although other species in solution above pH = 8.3 contribute to the alkalinity, e.g. $HSiO_3^-$, $NaHSiO_3$(aq), $CaCO_3$(aq), etc., the method of calculation is such that the true total HCO_3^- in solution can be approximated by the reported sum.

- An initial distribution of species at a reference temperature of 25°C using the given pH. The purpose of this calculation is to determine the charge imbalance, which includes those charged species resulting from hydrolysis. It is here assumed that the pH of the pore water was measured at this temperature in the laboratory immediately upon sampling.

Another useful check on the quality of the chemical analyses can be made by comparing the electrical conductivity computed from the chemical analysis of ionic species in solution with the measured electrical conductivity of that solution. This check was not performed in this study owing to time constraints, but has been evaluated empirically by Hem (1989).

The results of the above evaluation showed that the charge imbalances for many of the analyses were much larger than would be expected, i.e., ≤ 10 percent of the mean charge,

given the expected precision and accuracy of the analytical methods used. Apps (1997), in reviewing chemical analyses of J-13 well water (Harrar et al., 1990) concluded that the uncertainty in the measured pH values was so large that the reliability of the reported pH values of the pore waters might be questioned. Yang (1998, personal communicatoin) in responding to this query has indicated that several pH measurements were made during the recovery of a pore water sample from a drill core, and that the pH values reported were of the initial measurements. Because the pore waters are commonly quite alkaline, they tend to absorb CO_2 from the atmosphere, and this may have occurred to pore waters in the core periphery during recovery and subsequent storage. Accordingly, Yang has revised some of his reported pH measurements to reflect measurements on aqueous samples collected later in the pore water recovery process. These pH values are incrementally higher than those first reported.

In order to make an independent determination of the pH of the pore water, Apps (1997) assumed that the pore waters were just saturated with respect to calcite throughout all stratigraphic units. This assumption is supported by the presence of calcite in fractures throughout the vadose zone, except in the zeolitic interval of the Calico Hills Formation, where calcite is conspicuous by its absence, and which has been referred to as the "calcite barren zone" (Carey et al., 1997; Vaniman and Chipera, 1996). Furthermore, precipitation infiltrating Yucca Mountain may contact a caliche horizon and saturate with respect to calcite. Pore waters percolating through Yucca Mountain, if initially calcite saturated would, with one exception, tend to remain saturated as a result of rock and nitrate hydrolysis, and possibly evaporation. The exception occurs in the Calico Hills Formation, where zeolitic exchange of Ca^{++} and Mg^{++} for $2Na^{+}$ would tend to favor undersaturation, consistent with the above mentioned field observations indicating the absence of calcite in that zone.

The analyses of all pore waters were evaluated using EQ3 v. 7.2b with the constraint that the pH be adjusted to ensure calcite saturation. All runs were conducted at the estimated ambient temperature at which the core sample was collected in the borehole. Temperatures ranged from 17.5°C at the surface to 36.0°C at the maximum depth in borehole UZ-14. The temperatures were interpolated and calculated to ±0.1°C from either actual measured values or from values calculated for the Unsaturated Zone.

Results lead to a considerable improvement in the charge balance for most pore waters, particularly those whose pH was insufficiently high to record a measurable contribution from CO_3^{2-} and $HSiO_3^{-}$ to the alkalinity titration above pH = 8.3. In most cases the calculated pH was elevated with respect to the measured pH. However, for a significant number of analyses, particularly those with higher pH and alkalinity, the charge imbalance was not improved. In many cases, the charge imbalance remained between +10 and +30 percent of mean charge.

For those analyses reporting an alkalinity component above pH = 8.3, i.e., those analyses reporting CO_3^{2-}, it is possible to compute the pH independently of the measured pH, and without recourse to a calcite saturation constraint. Many of the analyses falling into this category were recovered from the Calico Hills Formation, where the absence of calcite in the matrix and high ion exchange potential would suggest possible undersaturation with respect to calcite. In order to calculate the pH from the alkalinity, the total alkalinity above pH = 8.3 must take into account the alkalinity contribution due to the dissociation of SiO_2(aq). Unfortunately, the qualified version of EQ3 is no longer equipped to make this correction (Wolery, 1992), and therefore it was made by graphical interpolation, assuming that the reported "CO_3^{2-}" actually comprises both CO_3^{2-} and $HSiO_3^-$. Other species contributing to the alkalinity, other than OH^- in the affected pore waters, generally affected the alkalinity above pH = 8.3 by only a few percentage points, i.e. ≤ 5 %.

Forty-five analyses reporting alkalinity above pH = 8.3 were accordingly corrected, and the pH and charge imbalance were calculated. Results lead to a considerable improvement in the charge imbalance, most showing imbalances of ≤10 percent. In most cases, however, calcite was supersaturated with saturation indices (SI = log (Q/K)) ranging from 0.0 to +1.2. This finding is inconsistent with the expectation that calcite would be undersaturated in the Calico Hills Formation, and challenges the presumption of calcite saturation (as opposed to supersaturation) in those pore waters where pH cannot be independently calculated from the alkalinity determination.

7.1.3 Preliminary Interpretation of Pore Water Equilibrium with Respect to Solid Phases

7.1.3.1 Calcite

Uncertainty regarding the state of calcite saturation within the vadose zone calls into question several assumptions inherent in the interpretation of the vadose zone geochemistry from the pore waters, in modeling of the thermochemical response of the DST, and in modeling the long-term behavior of the post-closure hydrochemical regime of the repository. Several possible explanations require further review, but until this issue is resolved, modeling the DST will be based on the assumption that calcite is initially saturated within the Tptpmn Unit, and that the kinetics of calcite precipitation are unaffected by other dissolved species. The following are potential explanations:

- Species sorbed on the surface of the calcite hinder precipitation. An abundant literature testifies to the supersaturation of solutions with respect to calcite in soils, e.g. see Suarez et al. (1992) and Levy et al. (1995). Lebron and Suarez (1996) have quite convincingly demonstrated that dissolved organic matter can greatly hinder the rate of precipitation at

soil temperatures, even at concentrations as low as 0.5 mg/L dissolved organic carbon (DOC). The total organic carbon concentration in water samples taken from 19 localities in the Yucca Mountain area between 1990 and 1992 (LaCamera and Westenburg, 1992) ranges from <0.1 to 1.5 mg/L. It is therefore possible that organic constituents inhibit calcite precipitation in the vadose zone at Yucca Mountain. It has long been known that calcite precipitation in seawater is hindered by the presence of Mg^{2+} (Mucci and Morse, 1983; Miyamoto and Pingitore, 1992), leading to the preferential precipitation of aragonite and/or high magnesium calcite. The pore waters at Yucca Mountain contain relatively high concentrations of Mg^{2+} (Yang et al., 1988, 1996a,b), but neither aragonite nor high magnesium calcite have been observed in either fractures or the matrix at Yucca Mountain; indeed, the calcite is reported to be almost pure (Carey et al., 1997). Amrhein (1998) suggested that $HSiO_3^-$ may adsorb on calcite surfaces and hinder precipitation. This potential explanation is attractive, because it would reconcile the presumed saturation of calcite at lower alkalinites with the calculated supersaturation of pore waters at higher alkalinites. It might also explain the observed absence of calcite in the "calcite barren zone" (Carey et al., 1997) as being due, not to undersaturation of calcite, but to inhibition of calcite precipitation. However, no experimental results exist to support this hypothesis. Other inhibiting aqueous species include phosphate ($H_2PO_3^-$) and fluoride (F^-). Both species are present at low concentrations (0.05 and 2.0 mg/L, respectively), and are less likely to be primary inhibitors.

- The omission of Ca complexes from the EQ3 DATA0 database. At present, no dissociation constants are present in the database for the species $CaSiO_3^-$, or $CaHSiO_3^+$. Such species might be significant in alkaline solutions at pH ≥ 9.0. They would depress the activity of Ca^{2+} and lower the apparent supersaturation of calcite.

- Erroneous solubility product of calcite. Repeated determinations of the thermodynamic properties and solubility product of calcite have established a high degree of confidence in currently recommended values for the solubility product by Plummer and Busenberg (1982) and Nordstrom et al., (1990), which is incorporated in the DATA0 database. However, a review is certainly merited.

- Apparent supersaturation induced by pore water evaporation during air drilling or storage. Artifacts resulting from collection, storage, and sampling procedures cannot be discounted. Their evaluation and quantification in the absence of other monitoring methods is questionable.

7.1.3.2 Illite/smectite (I/S)

Carlos et al. (1995a,b) have reported the presence of illite/smectite in the matrix throughout most of the vadose zone in drill cores USW G-1, G-2, and G-3 at Yucca Mountain. The I/S ratio, which is a measure of the maximum temperatures to which I/S is subjected, has also been investigated. These ratios indicate that regions of the lower part of the vadose zone have been subjected to elevated (hydrothermal) temperatures since deposition over 10 million years ago. In response to a debate concerning the status of I/S as a single phase or as two phases, Garrels (1984) demonstrated that I/S should be treated as two distinct phases rather than one. This he illustrated with an activity diagram of $\log[K^+]/[H^+]$ versus $\log[SiO_{2(aq)}]$ showing the calculated phase boundaries of I/S with respect to coexisting minerals, and upon which he plotted well-characterized groundwater compositions known to co-exist with I/S assemblages. In Figure 7.2, the same activity diagram is plotted, including the phase boundary separating illite from smectite determined by Garrels from the ground water analyses. On this figure are also plotted the calculated parameters derived from EQ3 distributions of chemical analyses of perched waters from Yucca Mountain, as reported by Yang et al. (1996a).

The $\log[K^+]/[H^+]$ versus $\log[SiO_{2(aq)}]$ data clearly reflect the same trend recognized by Garrels (1984), although the slope of the phase boundary is slightly steeper. The increased steepness is entirely consistent with more recent estimates of stoichiometry of the I/S phase pair by Aja (1995) and Kulik and Aja (1997), i.e. $K_{0.29}(Mg_{0.26}Al_{1.74})(Al_{0.03}Si_{3.97})O_{10}(OH)_2$ and $K_{0.5}(Mg_{0.22}Al_{1.78})(Al_{0.28}Si_{3.72})O_{10}(OH)_2$ for K-smectite and illite, respectively. The scatter off the phase boundary into the illite field might also be explained by the increasing activity ratio of $[Mg^{2+}]/[H^+]^2$ in solution for those analyses, and reflects the fact that the I/S phase boundary is pseudo-trivariant at a given P and T. The exchangeable cation site in the smectite is probably occupied by $0.5Ca^{2+}$ and or Na^+ rather than by K^+ as is represented by the above equation, but Figure 7.2 suggests strongly that the compositions of the perched waters, and by inference, the pore waters, may in part be controlled by the I/S phase pair. Of particular relevance is the $SiO_{2(aq)}$ activity, which in many pore waters exceeds the saturation of cristobalite, one of the principal minerals of the divitrified welded tuffs. Mg^{2+} and Ca^{2+} may also display binary control by smectite and other secondary phase in the system, i.e. sepiolite and calcite. Further investigation of these supposed controls is in progress.

7.1.3.3 Sepiolite

Sepiolite and/or palygorskite is commonly associated with pedogenic calcite and opal-CT in southern Nevada and adjacent regions of the desert southwest (Gardner, 1972; Hay and Wiggins, 1980; Machette, 1985; McFadden and Tinsley, 1985), and has also been observed in saline lake bed deposits of the Amargosa desert (Khoury et al., 1982; Eberl et al., 1982).

Sepiolite and palygorskite have also been found lining fractures in the vadose zone at Yucca Mountain (Carlos et al., 1995a), although Carey et al. (1997) were not able to identify either of these phases on fracture surfaces exposed in the ESF. Stoessell (1988) conducted an extended solubility study of both sepiolite and kerolite at 25°C and correlated his measurements with earlier work at higher temperatures. His solubility product values were used in preference to those in the EQ3 DATA0 database to test whether sepiolite is close to saturation within the vadose zone. Preliminary results from UZ-14 and UZ-16 pore water data by Yang et al. (1996a,b) show that the pore waters are for the most part at or near saturation with respect to sepiolite in units above the Calico Hills Formation. However, the waters become strongly undersaturated with respect to sepiolite in the latter. As noted above, sepiolite + I/S may control $[Mg^{2+}]/[H^+]^2$, thereby explaining the substantial invariance of this parameter in UZ-14 above the Calico Hills Formation (Apps, 1997). Traces of sepiolite may be present within the volume of rock occupied by the DST and should therefore be included in the model as a potential reactant phase, although its persistence, even at boiling water temperatures, is equivocal.

7.2 Gas Chemistry

7.2.1 Carbon dioxide

It is expected that ambient $\log P_{CO2}$ (bar) before turning on the heaters in the DST will range from −2.5 to −3.5. The most likely value is about −3.5, in conformity with atmospheric conditions, because excavation of the ESF and DST facility has allowed the ingress of atmospheric carbon dioxide. Upon heating, $\log P_{CO2}$ could rise to near zero in the desiccation zone adjacent to the heaters, if the rock were to behave as a closed system. However, such a scenario is considered unlikely, and $\log P_{CO2}$ is not expected to rise appreciably above −1.5. The actual value depends on several hydrologic parameters that will require quantification as modeling proceeds.

7.2.2 Nitrous oxide

As discussed in Section 11 of this report, nitrous oxide could be generated in the dryout zone through the partial decomposition of nitrate, thus:

$$2NO_3^- = 2NO_2^- + O_2 \qquad (7.1)$$

$$2NO_2^- + 2H^+ = N_2O + H_2O + O_2 \qquad (7.2)$$

Because nitrate decomposition could cause the residual pore waters to become more alkaline and affect the release of carbon dioxide, it is worth monitoring for the presence of nitrous

oxide in the gas phase. The concentration is expected to be low, but has been detected in a borehole elsewhere at Yucca Mountain (ONC#1) at a concentration of approximately 500 ppmv (Stellavato and Montazer, 1998). Its detection and evolution over time would provide useful insights into the desiccation process and the evolution of the pore water chemistry during desiccation.

7.2.3 Hydrogen

Hydrogen can be released during the cataclasis of minerals in rocks. This process arises from the rupturing of Si-O-Si bonds and subsequent hydrolysis, thus:

$$\text{-Si-O-Si-} = \text{Si-O-} + \text{-Si-} \qquad (7.3)$$

$$H_2O + \text{-Si-} = \text{-O-Si-} + H_2 \qquad (7.4)$$

The evolved hydrogen would be a measure of the extent of cataclasis caused by induced thermomechanical stresses during heating. Although the quantity of hydrogen evolved will be small, and may not be detectable, it would be worth testing for this gas as a measure of cataclastic deformation.

7.2.4 Other species, e.g. HCl, NH_3, $B(OH)_3$

Calculations indicate that the concentrations of HCl, NH_3, NH_4Cl, and $B(OH)_3$ in the gas phase, surrounding the desiccation zone, would be negligible. Most NH_4^+ infiltrating Yucca Mountain is probably bacterially decomposed or taken up by plants in the root zone, and I/S clays probably take up that part which penetrates below the root zone. Therefore the concentration of NH_4^+ at the repository horizon is expected to be vanishingly small. This has recently been confirmed by Yang (1998, personal communication), and therefore the amount of NH_3 or NH_4Cl released to the atmosphere would also be negligible, even though the pore waters are alkaline. Similarly, the evolution of HCl to the gas phase will remain negligible, unless the pH of the pore waters were to become acid at the final stages of desiccation, where the pore waters would be highly saline and consist primarily of residual sodium potassium chloride. Even then, the total mass released would be negligible and be immediately re-absorbed by condensate.

Boric acid, $B(OH)_3$, would volatilize in the zone of desiccation, particularly as temperatures reached 200°C, and would condense with the condensate. It is possible that it would accumulate in the aqueous phase as refluxing occurs, and could be a measure of the extent of rock alteration. Therefore, the measurement of $B(OH)_3$ in solution during the course of the

DST may be a useful indication of rock alteration. Such monitoring should be explored on an experimental basis.

8. TOUGHREACT CODE: BASIS OF GEOCHEMICAL CALCULATIONS

The module TOUGHREACT has been developed by Tianfu Xu and Karsten Pruess at LBNL to model non-isothermal multiphase reactive transport (Xu et al., 1997). TOUGHREACT considers homogeneous and heterogeneous reactions for an arbitrary number of primary chemical species and minerals under equilibrium and kinetic conditions, including adsorption and cation exchange. Also considered is the transport of an arbitrary number of species such as CO_2 and O_2 in the gas phase at equilibrium with the aqueous solution. As further discussed below, it is assumed that the partial pressures of the gaseous species are relatively low, such that they do not affect the total gas pressure.

An important aspect of TOUGHREACT is that its core structure is the TOUGH2 code, enabling it to treat various geochemical processes in the framework of dual permeability/porosity, multiple interacting continua (MINC), and equivalent continuum formalisms for fractured porous media, along with the transport of water, air, and heat. The geochemical and transport calculation methods incorporated in TOUGHREACT are summarized below. These have been enhanced as part of this study to deal with boiling conditions such as those arising from the DST.

8.1 Geochemical and Mass-Transfer Calculations

The geochemical module incorporated in TOUGHREACT solves simultaneously a set of chemical mass-action and mass-balance equations to compute the extent of reaction and mass transfer between a set of given aqueous species, minerals, and gases at each grid block of the flow model. Details on the coupling between the flow model (TOUGH2) and the geochemical module are described by Xu et al. (1997). Equations for flow and chemical reactions are solved sequentially rather than in a coupled fashion (e.g. Steefel and Lasaga, 1994). This sequential approach has proven to be more time- and memory-efficient than a fully-coupled formulation for problems of large size such as the 2-D and 3-D realizations needed for the Yucca Mountain Project.

The setup of mass-action and mass-balance equations in the geochemical module of TOUGHREACT is, in general, similar to the formulation implemented in other geochemical models (e.g. Reed, 1982; Wolery, 1992; Kharaka et al., 1988; Parkhurst et al., 1980; Ball and Nordstrom, 1991; Allison et al., 1991), with additional provisions for mineral dissolution and

precipitation under kinetic constraints and a volume-dependent formulation for gas equilibrium, as described below. The chemical system is described in terms of primary aqueous species (the independent variables). Minerals, gases, and secondary aqueous species are defined in terms of reactions involving only the primary species. It can be shown that if the dispersivities of all aqueous species are assumed equal, only the transport of primary species (in terms of total dissolved concentrations) need to be considered to solve the entire reactive flow/transport problem (Steefel and Lasaga, 1994).

The system of non-linear equations describing chemical mass-balance and mass-action is solved by a Newton-Raphson iterative procedure. Activity coefficients of aqueous species are computed by an extended Debye-Hückel equation (e.g. Parkhurst, 1990). Activity coefficients of neutral species are currently assumed equal to one, and the activity of water is computed using a method by Garrels and Christ (1965). A more rigorous treatment of activity coefficients will be incorporated in future versions of the code.

Equilibration with mineral phases is computed by adding a mass-action equation, for each saturated mineral, into the system of non-linear equations as follows:

$$\log(K_i) = \log(Q_i) \tag{8.1}$$

where K_i denotes the equilibrium constant and Q_i the product of the ion activities in the reaction that expresses mineral i in terms of the primary aqueous species. A term representing the amount of primary aqueous species consumed or produced by equilibration of minerals is added to the mass-balance equation for each primary species involved in mineral reactions, and is solved simultaneously with the concentrations of all primary species.

Kinetically retarded mineral precipitation and dissolution reactions are implemented in the code by incorporating a rate law which is dependent on the magnitude of the saturation index (Q/K) of each considered mineral (Aagaard and Helgeson, 1982; Velbel, 1989) as follows:

$$r = \mathrm{sgn}[1 - Q/K]kS\left[1 - (Q/K)^m\right]^n \tag{8.2}$$

$$\text{and } k = k_0 \exp\left[-E_a / R(1/T(K) - 1/298.15K)\right] \tag{8.3}$$

where r is the mineral precipitation (negative) or dissolution (positive) rate, k, E_a, and S are the rate constant, activation energy, and reactive surface area, respectively, T is temperature, R the ideal gas constant and sgn is the sign function. We assume that the exponents m and n equal one. The effect of pH and other aqueous species activities on reaction rates is not considered.

Over a finite time step Δt, the change in the concentration of each primary species j due to mineral precipitation or dissolution under kinetic constraints is computed from the sum of the rates, r_i, of all j-containing minerals i as follows:

$$\Delta C_j = \Sigma r_i \Delta t \qquad (8.4)$$

These concentration changes are incorporated into the mass-balance equation of each primary species involved in mineral reactions, using Equations (8.2) and (8.3), and solved simultaneously with the concentrations of all primary species (i.e. the ΔC_j terms are included into the jacobian matrix rather than computed externally). Instead of adding a separate rate equation for each mineral in the jacobian matrix, ΔC_j in terms of Equation (8.2) substituted in (8.3) is added to each mass-balance equation. Therefore, the size of the jacobian matrix does not increase with the addition of minerals to the system, in contrast to the case when minerals are assumed to precipitate or dissolve at equilibrium.

Minor gas species such as CO_2 are included in the model as ideal mixtures of ideal gases in equilibrium with aqueous and mineral phases. A mass-action equation is added to the system of simultaneous equations for each saturated gas present, except for H_2O and air (the carrier gases) which are handled separately through the flow module in TOUGH2. The gas mass-action equation takes the form:

$$\log(K_i) = \log(Q_i) - \log(P_i) \qquad (8.5)$$

where K_i and Q_i are as defined for Equation (8.1) and P_i is the gas partial pressure. The latter is replaced with the ideal gas law,

$$P_i = n_i / V_g RT \qquad (8.6)$$

where n_i denotes the number of moles of gas species i, R is the ideal gas constant, T is temperature, and V_g is the gas total volume (all trace gas species and carrier gas). By expressing V_g in terms of the gas saturation s_g, the porosity of the medium ϕ, and the (fixed) volume of each grid block in the flow model V_{block}, equation (8.5) is rewritten as:

$$P_i = n_i / \left(V_{block} \phi s_g\right) RT \qquad (8.7)$$

The gas saturation is computed externally by TOUGH2 for the carrier gas (H_2O and air). Substitution of Equation (8.6) into (8.4) allows for solving the amount of trace gas species (n_i/V_{block}) together with the concentrations of all primary species.

The partial pressures of gas species calculated in this fashion are not fed back to TOUGH2 for solving the water and gas flow equations. Therefore, this calculation method is valid only for minor gases with partial pressures significantly lower than the total gas pressure (i.e. lower than the pressure of the carrier gas). For cases where the partial pressures of minor gases become significant, chemical equilibrium with the aqueous phase is computed correctly but the gas and water flow velocities computed by TOUGH2 are likely to be underestimated.

For saturated flow conditions (s_g = 0), the partial pressure of dissolved gases is computed directly through Equation (8.3) (i.e. $\log(P_i) = \log(Q_i / K_i)$).

Provisions for handling real mixing of real gases will be included in future versions of the code. For low gas pressures (near atmospheric) such as those prevailing in the unsaturated zone at Yucca Mountain, the effect of gas non-ideality is assumed to be negligible, especially when compared to other uncertainties inherent to modeling any subsurface processes (Section 10).

8.2 Transport Calculations

As mentioned above, if the dispersivities of primary and secondary aqueous species are assumed equal, only the transport of total dissolved components need to be considered to solve the entire reactive flow/transport problem (Steefel and Lasaga, 1994). This is the approach used in TOUGHREACT. Primary aqueous species and trace gases are transported by advection and diffusion using the water and gas velocity field computed by TOUGH2. Transport computations are carried out component by component using the same integral finite-difference approach as in TOUGH2 (Pruess, 1991). For this study, a sequential non-iterative approach (Xu et al., 1997) is used between the flow and reaction-transport modules.

9. MODEL AND CODE TESTING

As a recently developed code in which a wide range of physical phenomena and chemical processes are considered, it is important that verification and validation tests be made. In this section we present some of the important tests we have made for this project. At the current stage of this investigation, these tests should not be regarded as exhaustive. Other tests have been done by the primary authors of TOUGHREACT (Section 4.2) and will be presented for software QA. Further improvement and verification of TOUGHREACT is ongoing and, therefore, the results presented in this report are preliminary.

Several model simulations were performed to assess the results of the TOUGHREACT code for simulations of water-rock interaction under equilibrium and kinetic conditions. Equilibrium simulations were performed to compare the mineral assemblages and chemical compositions under "batch reactor" conditions to that given by the well-tested equilibrium code CHILLER (Reed 1982; Spycher and Reed, 1992). Kinetic simulations were compared to plug flow reactor experiments and model simulations on quartz and Topopah Spring welded tuff (Johnson et al., 1997a).

9.1 Equilibrium Simulations: Heating and Boiling without Advection/Dispersion

Simple computations using 1 and 2 grid blocks were performed to check gas, mineral, and aqueous phase equilibria in closed systems with no or limited advection/dispersion of chemical reactants. Heating and boiling simulations were conducted with TOUGHREACT and benchmarked against the results of CHILLER. CHILLER computes multicomponent chemical equilibria between an aqueous phase, minerals, and gases, and was specially designed for boiling and heating problems. CHILLER includes an option for incrementally adding heat into the chemical system to simulate boiling, which makes it practical for comparison with similar heat-"titration" simulations using TOUGHREACT.

A heating simulation was performed with TOUGHREACT using one grid block and fully saturated conditions. Heat was added to the water-only system to raise its temperature from 25 to 200°C. The pressure was maintained above the water saturation pressure so that no gas phase was formed. An equivalent simulation was conducted with CHILLER. For both cases, identical thermodynamic data bases were used: data from SUPCRT92 as reported by Johnson et al. (1992) upgraded with aluminum data from Pokrovskii and Helgeson (1995) (data compiled in SOLTHERM.JOH data base, courtesy of M.H. Reed, University of Oregon).

The composition of the water for this benchmarking exercise was taken from Yang et al. (1996a) (Sample UZ-16 at 1296.8 feet depth). The simulations were set to maintain equilibrium with calcite, albite, k-feldspar, kaolinite, and cristobalite. Two other minerals, sepiolite and anhydrite, were allowed to precipitate. No other minerals were allowed to form.

Results are shown on Figure 9.1, where output data from TOUGHREACT are shown with solid lines and CHILLER results are shown with symbols. The aqueous phase compositions and CO_2 fugacities computed by both programs are in very good agreement. The same is true for precipitated (positive) and dissolved (negative) mineral amounts. There is a small divergence in computed calcite amounts between 50 and 150° C (exaggerated by a factor of 100 on Figure 9.1a). This divergence does not affect the computed concentrations of aqueous species. It may be related to a difference in residual error in the carbonate mass

balance (the calcite amount is quite small) and possibly also to a difference in computed activity coefficient for calcium and/or carbonate species as a function of temperature.

Benchmark boiling simulations were accomplished with the same water composition and mineral assemblage as for the heating test. Heat was incrementally added into the initially saturated (no gas) solution at 100°C, but this time the pressure was maintained near 1 atmosphere to allow a gas phase to form. In this case, the CHILLER and TOUGHREACT simulations were more difficult to benchmark because CHILLER computes boiling using pressure (with volume undefined, thus variable) while TOUGHREACT uses a fixed volume. Variable volume simulations were approximated with TOUGHREACT by setting a two-block grid, with one of the blocks representing the initially saturated (no gas) solution, and the other block set with a very large volume filled mostly with air. At a pressure near 1 atmosphere and temperature of 100°C, heat was "titrated" into the first block to simulate boiling, with the gas phase expanding into the second block, and pressure remaining constant because of the large volume of this block.

Results of both simulations are shown on Figures 9.2 through 9.4. These figures were plotted with the X-axis representing heat increasing from left to right, thus showing temperature increasing until the onset of boiling (100°C), then the boiling weight fraction at the constant temperature of 100°C (pressure is maintained near 1 atm.). The CHILLER simulation reveals a more pronounced effect from early CO_2 degassing than the TOUGHREACT simulation (Figure 9.2). This results in a CO_2 pressure trend and a final pH different from those computed with TOUGHREACT, as well as a more pronounced effect on mineral dissolution and precipitation amounts (Figure 9.3). However, both simulations show consistent aqueous chemistry trends with a similar evaporative concentration trend for chloride (a useful conservative tracer in this case) (Figure 9.4). The simulations also indicate similar mineral precipitation and dissolution trends, including the precipitation of anhydrite at the later stages of boiling (Figure 9.3). The greater CO_2 degassing effect in the CHILLER simulation may be related to the absence of a volume constraint in the calculation method (closed system with expanding volume) and likely also to the different activity coefficient calculation methods incorporated in each program.

TOUGHREACT results show a lesser CO_2 degassing effect, with CO_2 pressures still slightly increasing after the onset of boiling. These results could be representative of a case where an extreme CO_2 degassing effect may not occur due to the ubiquitous presence of atmospheric CO_2.

9.2 Kinetic Simulations of Plug Flow Reactor Experiments

Details of the plug flow reactor experiments on quartz and tuff, and GIMRT simulations, can be found in Johnson et al., (1997a). Here we describe the most important aspects to be considered for modeling conditions, and to compare to TOUGHREACT results.

9.2.1 Quartz

This experiment used crushed quartz grains having a range in grain size from 75 to 125 μm, packed in a tube 3.1 cm in length and of inside diameter 0.66 cm. The temperature was held constant at 239° C and the average flow rate measured over the duration of the experiment (12.7 days) was 24.8 mm/day, under saturated flow conditions. The inlet fluid was distilled water. The initial porosity was not known exactly, and an average of values from 40 to 45% was given as 42.5%.

The outlet concentration of Si reached a roughly constant value of 105.4 ppm before the first measurement was made (16.2 hours). Because the equilibrium concentration of Si in equilibrium with quartz at 239° C is 156.8 ppm, the experiment can be considered as pure dissolution under kinetic conditions (Johnson et al., 1997a).

The latter authors also presented results of GIMRT (Steefel and Yabusaki, 1996) simulations, assuming a constant flow field. The average outlet concentration in the experiment was best matched using the kinetic data given by Tester et al. (1994) and using a calibrated reactive surface area of between 335 and 368 cm^2/g for an initial porosity range of 40 to 45%. For comparison, Johnson et al. (1997a) reported a BET measured surface area range from 368 to 650 cm^2/g.

A 1-D TOUGHREACT simulation was performed using a 31 volume element mesh with dimensions and interface areas identical to that of the plug flow experiment, plus one boundary element to set the appropriate outlet conditions. A constant injection rate (mass flux) was applied corresponding to the volume flux of 24.8 mm/day at 239° C, calculated using an estimated density[1] of 0.817 g/cm^3. The permeability of the packed quartz grains was not given, and was therefore calculated assuming a cubic array of truncated spheres (Weyl, 1959) having a grain size of 100 μm with a truncation factor set to that needed to yield a porosity of about 42.5% (~ 0.97). A permeability of 6.51×10^{-12} m^2 was calculated from the minimum pore throat diameter and number of pores per unit area of this grain texture using the modified Hagen-Poiseulle equation as described by Ehrlich et al. (1991). The kinetic rate for dissolution adopted was 0.2724×10^{-7} mol/ m^2s as derived from Tester et al. (1994), and used by Johnson et al., (1997a).

[1] The fluid density was calculated using the temperature dependence given by Person and Garven (1992), and assuming a typical linear compressibility of pure water as 4.522×10^{-5} bar^{-1}.

The results of this simulation are close to that given by Johnson et al. (1997a). Using a specific surface area of 350 cm^2/g which is approximately the best fit surface area from Johnson et al. (1997a) we obtain an outlet concentration of 104 ppm Si, as compared to the 105.4 ppm measured in the experiment. The average porosity at the end of the simulation was 44.68%, compared to 44.55% found by Johnson et al. (1997a).

9.2.2 Topopah Spring Tuff

The experiment on Topopah Spring welded tuff, described by Johnson et al. (1997a), consisted of crushed tuff in a tube of length 26.3 cm and diameter 0.66 cm. The experiment was run for 36 days at a constant temperature of 240° C and an average flow rate of 25 ml/day. The initial porosity was estimated to be 42.5%. Roughly steady-state concentrations were attained after about a day, although there was a general decline in Si (aq) over time.

The mineral assemblage used in the TOUGHREACT and GIMRT simulations was quartz, cristobalite (α), amorphous silica, K-feldspar, albite, anorthite, kaolinite, paragonite, muscovite, gibbsite, boehmite, diaspore, and pyrophyllite. Except for anorthite, the same dissolution rate constants as those presented in Johnson et al. (1997a) were employed. The rate constant given for the anorthite component was several orders of magnitude greater than for the k-feldspar and albite components, and given that the calcium is in solid solution with the other feldspars (predominantly in exsolved albite) the rate was adjusted to the same order of magnitude as albite. The same surface areas for dissolution were used; however, the GIMRT code incorporates a relation of precipitation surface area to porosity that is not implemented in TOUGHREACT, so that the precipitation kinetics are different. For this reason, and differences in thermodynamic data, the results can only be compared qualitatively.

Here, we compare the measured outlet concentrations to the TOUGHREACT and GIMRT simulations. We compare the results at approximately 22 days, instead of 36 days, because this corresponds approximately to the maximum number of time steps that TOUGHREACT reached before the final simulation time of 36 days. Because the simulation concentrations do not change over time (no phase was exhausted and there is no feedback to the flow field in terms of porosity or permeability changes), the shorter time period makes no difference in the results.

Table 9.1 shows the outlet concentrations from the experiment and the model simulations. The first two TOUGHREACT (TR-1 and TR-2) simulations show the effect of changing from the original thermodynamic database used in TOUGHREACT that is derived from SUPCRT92 (TR-1) to the updated database presented in this report (TR-2). The third simulation (TR-3) illustrates the effect of suppressing quartz precipitation, as was indicated

by the lack of quartz precipitates in the experiment, and the known difficulty for quartz nucleation (Rimstidt and Barnes, 1980).

Table 9.1. Comparison of measured outlet concentrations from a TSw tuff plug flow reactor experiment and GIMRT simulation (Johnson et al., 1997a) and TOUGHREACT simulations.

Cation	Meas. (ppm)	GIMRT-A	TR - 1	TR - 2	TR - 3
Si	356.951	252.17	191.9	186.9	309.2
Na	14.003	9.76	30.1	27.3	16.8
K	2.253	1.09	3.36	3.03	1.86
Ca	0.043	0.0103	0.044	0.036	0.089
Al	7.17	7.03	8.36	6.90	2.21

Although the TOUGHREACT results are not identical to GIMRT outlet concentrations, the analysis shows that the model describes the experimental data as well as GIMRT. Differences in the cation ratios in the output fluid are due mainly to the different precipitation kinetics employed for the secondary phases.

10. DATA UNCERTAINTIES

Any modeling of heat and fluid flow in the subsurface is subject to large uncertainties resulting from the inherently heterogenous nature of subsurface materials. In addition, calculation methods and assumptions also contribute to the uncertainty of modeling results. For coupled flow and reactive transport simulations, this uncertainty is compounded by the fact that the simulations rely largely on the thermodynamic and kinetic data input into the model. These include the dissociation constants K in Equations 8.1 and 8.2, and rate constants, activation energies, and very uncertain surface areas in Equation 8.2. The calculation methods and parameters used for computing activity and fugacity coefficients also affect modeling results. All these data have significantly large uncertainties which directly affect modeling results.

The mineral saturation indices (log [Q/K]) determine whether a mineral precipitates or dissolves either at equilibrium (Equation 8.1) or under kinetic constraint (Equation 8.2). To provide an example of the effect of log(K) data on computed saturation indices, simple speciation calculations were performed using thermodynamic data from two commonly used data bases: Johnson et al., (1992) (SUPCRT92) with revised aluminum data by Pokrovskii and Helgeson (1995), and data from Holland and Powell (1990) (compiled data in SOLTHERM.JOH and SOLTHERM.HP databases, courtesy of M.H. Reed, University of Oregon). Saturation indices were computed with SOLVEQ (Reed, 1982) for several minerals from 25 to 200°C and the same water composition as for the tests described in Section 9.1.

Differences between computed Q/K values were up to a several orders of magnitude for many alumino-silicate minerals. For two common rock forming minerals at Yucca Mountain, albite and K-feldspar, log (Q/K) differences up to 1 and 0.7, respectively, were calculated. Similar conclusions on the discrepancy between thermodynamic data for these minerals have been expressed by Apps and Chang (1992).

The uncertainty of published kinetic data for many minerals is even greater than for dissociation constants, which compounds the uncertainty on reaction rates expressed through Equation (8.2). Only careful experimental and field studies combined with modeling (such as in the plug flow experiments) will allow refinement of thermodynamic controls and the effective rates of reaction.

11. EXPLORATORY GEOCHEMICAL SIMULATIONS

In this section, we discuss the results of a series of preliminary simulations of chemical processes in the DST in either the dryout (desiccation) zone immediately surrounding the heaters or in the region of condensation. These simulations allow a conceptual understanding of the chemical evolution of a system as a function of some specified physical or chemical variable. This variable can be a reaction progress parameter, such as the extent of evaporation, boiling or cooling, or some externally defined chemical potential, such as the partial pressure of carbon dioxide, which can be varied over a range realistically expected during the course of the DST. The advantage of such simulations is that they are easy to perform, and facilitate interpretation of more complex THC simulations involving both spatial and temporal domains.

The section comprises two separate studies. The first is made using EQ3 v7.2b, a qualified distribution-of-species code. The code is used to conduct simple calculations to study the chemical behavior of the residual brine during evaporation in the desiccation zone, assuming partial equilibrium with the host rock minerals. The code is also used to evaluate condensate chemistry as a function of variable ambient partial pressure of carbon dioxide. In the second section, more ambitious reaction progress simulations are conducted using the unqualified code CHILLER, which is advantageously configured to permit studies of the evolution of systems during either boiling or condensation.

The results of the two sets of simulations are broadly comparable, after due consideration is given to differences in the way in which the simulations were conducted, and minor differences in model assumptions.

11.1 Thermochemical Processes of the Altered Zone

11.1.1 Zone of Desiccation

In the zone immediately adjacent to the waste containers or surrogate waste (electric heaters), temperatures are expected to rise to a maximum of 200°C. This will lead initially to boiling of the rock pore water, and eventually to complete evaporation and drying. Because the pore water is relatively dilute, the initial boiling temperature will be at approximately the temperature at which pure water boils at the elevation of the ESF, i.e., approximately 95°C. With progressive concentration of residual salts, the temperature will rise, until crystallization of the dissolved residue and complete desiccation takes place. Between 95 and 200°C, some dehydration of small quantities of smectite in illite/smectite (I/S) assemblages may occur, and decomposition of calcite precipitates is possible. However, both such processes are expected to be minor.

In order to provide an initial scoping of the chemical processes in the zone of desiccation, a series of calculations were conducted to determine potential precipitates likely to be observed during boiling and the equilibrium partial pressure of carbon dioxide at various stages of concentration[2]. Two sets of simulations were made. The first assumes that no carbon dioxide is released from the pore water during concentration, i.e. the system is considered closed, and the second assumes that the partial pressure of carbon dioxide is controlled externally at 10^{-2} bar, i.e. the system is considered open with respect to P_{CO2}. Furthermore, it is assumed in both cases that calcite, cristobalite, high albite, sanidine, and sepiolite are initially at saturation and remain so. The assumed phase saturations are based on a preliminary assessment of thermodynamic controls on the pore water composition at Yucca Mountain (Apps, 1997), on the assumption that the primary mineral products of devitrification are cristobalite and sanidine, and that cristobalite, high albite and sanidine are convenient end-member phases present in the EQ3/6 v.7.2b database. However, evidence from a transmission electron microscope study of a divitrified tuff similar in provenance and composition to that of the TSw units at Yucca Mountain suggests that the sanidine laths in the axiolitic and spherulitic intergrowths of the welded units may have recrystallized to potash feldspar (microcline?) and low albite (Tarshis, 1982).

The two simulations represent the extremes of closed versus open systems. In reality, the desiccating zone will likely remain partially open, depending on a variety of complex hydrological and hydrochemical factors, quantifiable only with non-isothermal reactive

[2] EQ3 V. 7.2b (Wolery, 1992) was employed in the calculations using the unmodified database issued with the code. The database requires modification to be suitable for application to problems germane to the DST and subsequent modeling of the proposed waste repository hydrogeochemistry. Modeling results are therefore preliminary.

chemical transport modeling of the vadose zone at Yucca Mountain, as well as the acquisition of new data from the DST.

The initial conditions are summarized in Table 11.1, and the results are presented graphically in Figures 11.1, 11.2 and 11.3. Figure 11.1 displays the evolution of the principal chemical constituents of the pore water as a function of the concentration factor due to boiling. Significant differences in chemistry between open and closed systems occur with respect to Mg, Ca, and HCO_3^-. In the closed system, the concentration of Mg increases sharply with boiling, as the solubility of sepiolite increases with declining pH, as shown in Figure 11.2. This suggests that sepiolite would dissolve, releasing SiO_2(aq) and Mg^{2+} to the solution. The Mg^{2+}, in turn, would contribute to the precipitation of secondary smectite. HCO_3^- in the closed system increases in conformity with concentration due to evaporation, depressing the Ca concentration in relation to the open system. In Figure 11.2, the corresponding variations in pH and P_{CO2} are recorded. In the closed system, P_{CO2} rises dramatically with concentration of dissolved salts, attaining approximately one bar (10^5 Pa) with a 16 fold concentration. The pH in both cases declines with evaporation, but the closed system pH falls further, as would be expected. These results do not take into account the possible dilution of CO_2 by steam in an open system, which could lead to transient declines in P_{CO2} and positive pH excursions. These results differ from preliminary TOUGHREACT simulations presented in this report.

Table 11.1 EQ3 Modeling of Evaporation at 100°C

Constituent	Initial Composition (mg/L)	Constraint (Closed)	Constraint (Open)
H^+	-	UEBAL[1]	UEBAL
Na	9.	Conc.Factor	Conc. Factor
K	-	Sanidine high	Sanidine high
Mg	12.	Sepiolite	Sepiolite
Ca	65.	Calcite	Calcite
Al	-	Albite high	Albite high
SiO_2(aq)	46.	Cristobalite (beta)	Cristobalite(beta)
HCO_3^-	66.	Conc. Factor	Conc. Factor
SO_4	79.	Conc. Factor	Conc. Factor
Cl	77.	Conc. Factor	Conc. Factor
NO_3	12.	Conc. Factor	Conc. Factor

[1]VEBAL indicates that selection of ionic species used to achieve electrical neutrality in the aqueous phase.

Figure 11.3 indicates that the specified mineral assemblage is unstable with respect to calcium montmorillonite, and that the boiling stage would enhance the decomposition of the primary minerals to form secondary clays. Under open system conditions, anhydrite ($CaSO_4$) is also likely to precipitate after the pore waters have evaporated to less than one quarter their

initial volume. The total quantity of anhydrite, however, will be negligible, and would not have a significant effect on the porosity or permeability of the devitrified tuff matrix.

Thin section descriptions by Broxton et al. (1982) of the welded devitrified tuffs at Yucca Mountain suggest that "clay" (presumably illite/smectite) may be in part due to the alteration of extremely fine axiolitic or spherulitic sanidine/cristobalite intergrowths. It is possible that the excess free energy contribution imparted by the enhanced surface area of these intergrowths destabilized them in favor of coarser intergrowths. However, a more critical examination will be needed to clarify this matter. The rate of alteration of the primary feldspars and cristobalite in the rock could be dependent on the specific surface area, which varies depending on the coarseness of the primary and secondary mineral textures. Because the rate of alteration of the welded tuffs is estimated to be only of the order of 1 to 10×10^{-9}/yr., or a few percent of the rock over a ten million year period, (Johnson and DePaolo, 1994), the extent of alteration to clay before desiccation of the inner thermal zone within four years is not expected to increase by more than a factor of two. Recognition of such alteration during the course of the DST is expected to be subtle, and will require perseverance in its identification.

The potential precipitation of small amounts of anhydrite and residual salts in DST desiccation zone samples will likewise be difficult to discern by optical methods. Thus, alteration of this zone is expected to be trivial over the lifetime of the DST test. Under actual proposed repository conditions, longer duration thermal alteration will cause dehydration of the small amounts of clay minerals present, i.e., I/S and sepiolite, and decarbonation of calcite. The latter processes will be of minor consequence because of the small concentrations of participating minerals.

Although the above simulations are believed to be reasonable, there exists the possibility that elevated temperatures may accelerate nitrate decomposition according to the following equations (Cooper and Smith, 1963; Mehran and Tanji, 1974):

$$2NO_3^- = 2NO_2^- + O_2 \qquad (11.1)$$

$$2NO_2^- + 2H^+ = N_2O + H_2O + O_2 \qquad (11.2)$$

$$2N_2O + 2N_2 + O_2 \qquad (11.3)$$

In sum:

$$2NO_3^- + 2H^+ = N_2 + 2.5O_2 + H_2O \qquad (11.4)$$